Electronic Supporting Information

Dual-Binding Conjugates of Diaromatic Guanidines and Porphyrins for Recognition of G-Quadruplexes

Jagdeep Grover,[a] Cristina Trujillo,[a] Mona Saad,[b] Ganapathi Emandi,[a] Nikolina Stipaničev,[a] Stefan S. R. Bernhard,[a] Aurore Guédin,[b] Jean-Louis Mergny,[b] Mathias O. Senge,[a] and Isabel Rozas[a,*]

E-mail: rozasi@tcd.ie

Contents

Experimental Section S2
Chemistry S2
General conditions S2
General procedure for the preparation of Boc-protected porphyrin-guanidine conjugates (**2a-f**) S2
General procedure for preparation of hydrochloride salts (**3a-f**) S4
General procedure for porphyrin metallation (**4a** and **4e**) S5
Biophysical studies S7
Oligonucleotides S7
UV-Thermal Melting Experiments S7
FRET melting assay S9
Circular dichroism (CD) spectroscopy S11
UV-Vis titration studies S12
Modelling studies S20
Purity assessment of final compounds S31
^{1}H and ^{13}C NMR Spectra of new compounds S35
References S48

Experimental Section

Chemistry

General conditions

All commercial chemicals were obtained from either Sigma-Aldrich or Fluka and used without further purification. Deuterated solvents for NMR spectroscopy use were purchased from Apollo. Column chromatography was performed using Sigma-Aldrich silica gel 100-200 mesh. Solvents for synthesis purposes were used at GPR grade. Analytical TLC was performed using either Merck Kieselgel 60 F254 silica gel plates or Polygram Alox N/UV254 aluminium oxide plates. Visualization was by UV light (254 nm). NMR spectra were recorded on Bruker DPX-400 Avance spectrometers, operating at 400.13 and 600.1 MHz for ^{1}H NMR; 100.6 and 150.9 MHz for ^{13}C NMR. Shifts are referenced to the internal solvent signals.[1] NMR data were processed using BrukerTOPSPIN software. HRMS spectra were measured on a MicromassLCT electrospray TOF instrument with a WATERS 2690 autosampler and methanol/acetonitrile as carrier solvent. Melting points were determined using a Stuart SP10 melting point apparatus and are uncorrected. Infrared spectra were recorded on a PerkinElmer Spectrum One FT-IR spectrometer equipped with a Universal ATR sampling accessory. UV-Vis spectra were recorded on Specord 250 spectrophotometer in the 200–700 nm range at 25 °C with a 1 cm path-length quartz cell.

*General procedure for the preparation of Boc-protected porphyrin-guanidine conjugates (**2a-f**)*

For the synthesis of intermediates (**2a-f**), we commenced with preparation of starting materials *para*-amino tetraphenylporphyrin (***p*-NH$_2$-TPP**) and 4,4'-bis-Boc-protected guanidines (**1a-f**). ***p*-NH$_2$-TPP** was synthesized following the literature method starting from 5,10,15,20-tetraphenylporphyrin followed by mononitration (using sodium nitrite and trifluoroacetic acid) and subsequent reduction.[2] The synthesis of **1a-f** was achieved by guanidylation of 4,4'-dianilines using the well-established protocol of our laboratory.[3] To a stirred solution of ***p*-NH$_2$-TPP** (0.3 mmol) in $CHCl_3$ (6-7 mL), was added **1a-f** (1.2 equiv.) and resulting reaction mixture was refluxed for 24 h. The progress of reaction was monitored by TLC. Upon completion, the excess solvent was evaporated under vacuum and further purification was done using column chromatography (eluted in hexane:DCM, 60:40). The intermediate **2d** was not purified owing complex mixture with Boc-deprotected conjugates, so used as such for Boc-deprotection.

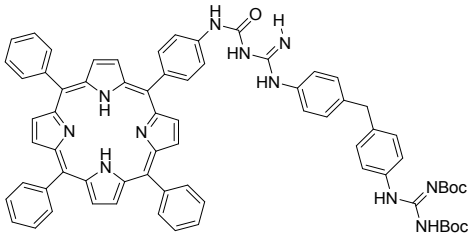

2a: Yield = 47%. m.p. >300 °C. R_f = 0.5 (hexane/EtOAc = 8/2). **^{1}H NMR** (400 MHz, $CDCl_3$): δ. 12.25 (s, 1H, NH), 11.66 (s, 1H, NH), 10.32 (s, 1H, NH), 10.29 (s, 1H, NH), 8.90 (d, *J* = 4.6 Hz, 2H), 8.86 (s, 6H), 8.24 (d, *J* = 6.4 Hz, 6H), 8.17 (d, *J* = 8.0 Hz, 2H), 7.89 (d, *J* = 7.8 Hz, 2H), 7.78-7.76 (m, 9H), 7.59 (d, *J* = 8.0 Hz, 4H), 7.47 (s, 1H, NH), 7.25-7.20 (m, 4H), 4.00 (s, 2H, CH_2), 1.60 (s, 9H, $(CH_3)_3$), 1.55 (s, 9H, $(CH_3)_3$), 1.52 (s, 9H, $(CH_3)_3$), -2.72 ppm (s, 2H). **^{13}C NMR** (100 MHz, $CDCl_3$): δ. 163.6, 162.5, 153.5, 153.4, 153.3, 152.6, 142.2, 138.5, 137.9, 137.4, 136.9, 135.1, 135.0, 134.9, 134.5, 129.4, 129.3, 127.7, 126.7, 122.9, 122.4, 122.3, 120.1, 120.0, 117.4, 83.7, 83.5, 79.6, 40.8 ppm. **HRMS** (ESI): *m/z* Calcd. for $C_{75}H_{71}N_{11}O_7$ $(M)^+$: 1237.5538, Found: 1237.5582.

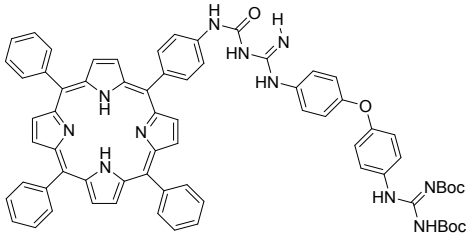

2b: Yield = 55%. m.p. >300 °C. R_f = 0.6 (hexane/EtOAc = 8/2). **^{1}H NMR** (400 MHz, $CDCl_3$): δ. 12.23 (s, 1H, NH), 11.64 (s, 1H, NH), 10.31 (s, 1H, NH), 10.26 (s, 1H, NH), 8.89 (d, *J* = 4.6 Hz, 2H), 8.82 (s, 6H), 8.20 (d, *J* = 6.9 Hz, 6H), 8.14 (d, *J* = 8.1 Hz, 2H), 7.86 (d, *J* = 7.9 Hz, 2H), 7.78-7.72 (m, 9H), 7.60 (d, *J* = 8.8 Hz, 4H), 7.47 (s, 1H, NH), 7.07-7.02 (m, 4H), 1.57 (s, 9H, $(CH_3)_3$), 1.53 (s, 9H, $(CH_3)_3$), 1.49 (s, 9H, $(CH_3)_3$), -2.77 ppm (s, 2H). **^{13}C NMR** (100 MHz, $CDCl_3$): δ. 163.5, 162.5, 154.6, 154.0, 153.5, 153.4, 142.2, 138.4, 136.9, 135.1, 134.5, 132.3, 132.0, 131.2, 131.1, 130.9, 127.6, 126.7, 126.6, 124.3, 123.8, 120.0, 119.98, 119.92, 119.3, 118.9, 117.4, 83.7, 83.5, 79.6, 28.2, 28.1, 28.0 ppm. **HRMS** (ESI): *m/z* Calcd. for $C_{74}H_{70}N_{11}O_8$ $(M+H)^+$: 1240.5409, Found: 1240.5403.

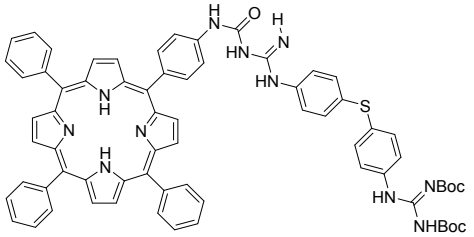

2c: Yield = 52%. m.p. >300 °C. R_f = 0.5 (hexane/EtOAc = 8/2). **^{1}H NMR** (400 MHz, $CDCl_3$): δ. 12.24 (s, 1H, NH), 11.64 (s, 1H, NH), 10.41 (s, 1H, NH), 10.38 (s, 1H, NH), 8.91 (s, 2H), 8.84 (s, 6H), 8.20 (d, *J* = 6.0 Hz, 6H), 8.16 (d, *J* = 7.7 Hz, 2H), 7.89 (d, *J* = 7.2 Hz, 2H), 7.76-7.74 (m, 9H), 7.63 (d, *J* = 8.0 Hz, 4H), 7.49 (s, 1H, NH), 7.38-7.36 (m, 4H), 1.58 (s, 9H, $(CH_3)_3$), 1.53 (s, 9H, $(CH_3)_3$), 1.51 (s, 9H, $(CH_3)_3$), -2.74 ppm (s, 2H). **^{13}C NMR** (100 MHz, $CDCl_3$): δ.163.4, 162.3, 153.45 (2C), 153.41, 152.4,142.2, 138.4, 137.0, 136.3, 135.9, 135.1, 134.5, 132.2, 131.1, 131.0, 127.6, 126.6, 123.1, 122.8, 120.1, 120.0, 119.9, 117.5, 83.9, 83.6,

79.8, 28.2, 28.13, 28.0. **HRMS** (ESI): *m/z* Calcd. for $C_{74}H_{69}N_{11}O_7SNa$ $(M+Na)^+$: 1278.5000, Found: 1278.5092.

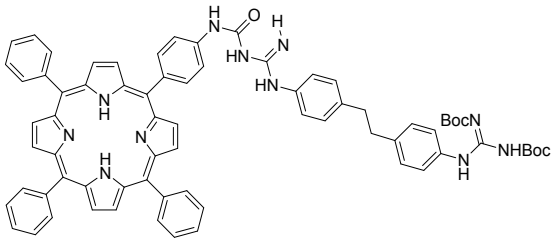

2e: Yield = 62%. m.p. >300 °C. R_f = 0.5 (hexane/EtOAc = 8/2). **^{1}H NMR** (400 MHz, $CDCl_3$): δ. 12.23 (s, 1H, NH), 11.64 (s, 1H, NH), 10.28 (s, 2H, NH), 8.89 (d, *J* = 4.7 Hz, 2H), 8.83 (s, 6H), 8.20 (d, *J* = 6.5 Hz, 6H), 8.14 (d, *J* = 8.1 Hz, 2H), 7.86 (d, *J* = 7.8 Hz, 2H), 7.78-7.72 (m, 9H), 7.57-7.52 (m, 4H), 7.45 (s, 1H, NH), 7.21 (d, *J* = 8.1 Hz, 2H), 7.15 (d, *J* = 7.8 Hz, 2H), 2.92 (s, 4H), 1.57 (s, 9H, $(CH_3)_3$), 1.52 (s, 18H, $(CH_3)_3$), -2.76 ppm (s, 2H). **^{13}C NMR** (100 MHz, $CDCl_3$): δ.163.6, 162.6, 153.5, 153.4, 153.3, 152.6, 142.2, 138.6, 138.5, 138.1, 136.9, 135.1, 134.8, 134.5, 128.9, 127.7, 126.6, 122.7, 122.2, 120.1, 120.0, 119.9, 117.4, 83.6, 83.5, 79.5, 37.4, 37.3, 28.2, 28.17, 28.12 ppm. **HRMS** (ESI): *m/z* Calcd. for $C_{76}H_{73}N_{11}O_7$ $(M)^+$: 1251.5694, Found:1251.5673.

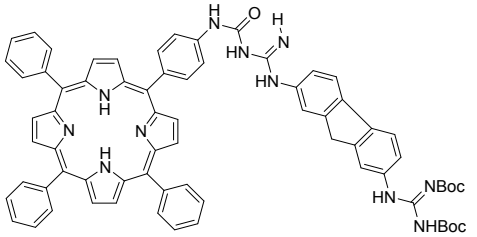

2f: Yield = 65%. m.p. >300 °C. R_f = 0.6 (hexane/EtOAc = 8/2). **^{1}H NMR** (400 MHz, $CDCl_3$): δ. 12.27 (s, 1H, NH), 11.69 (s, 1H, NH), 10.47-10.41 (m, 2H, NH), 8.89 (d, *J* = 4.4 Hz, 2H), 8.83 (s, 6H), 8.20 (d, *J* = 6.2 Hz, 6H), 8.15 (d, *J* = 7.9 Hz, 2H), 7.95 (s, 1H), 7.87 (d, *J* = 7.9 Hz, 3H), 7.75-7.73 (m, 11H), 7.53-7.50 (m, 2H), 3.98 (s, 2H), 1.58 (s, 9H, $(CH_3)_3$), 1.54 (s, 18H, $(CH_3)_3$), -2.76 ppm (s, 2H). **^{13}C NMR** (100 MHz, $CDCl_3$): δ. 163.6, 162.6, 153.54, 153.52, 153.4, 152.7, 144.2, 142.23, 142.22, 138.5, 138.0, 136.9, 135.5, 135.3, 135.1, 134.5, 127.6, 126.6, 121.8, 121.0, 120.1, 120.0, 119.9, 119.8, 119.7, 119.6, 119.0, 117.4, 83.7, 83.5, 79.7, 37.2, 28.2, 28.17, 28.12 ppm. **HRMS** (ESI): *m/z* Calcd. for $C_{75}H_{69}N_{11}O_7$ $(M+H)^+$: 1235.5381, Found: 1235.5442

*General procedure for preparation of hydrochloride salts (**3a-f**)*

To Boc-protected guanidine precursors (**2a-f**, 1.0 equiv.) were added 4 M HCl/1,4-dioxane (6.0 equiv. per Boc group) and $CHCl_3$ (2-3 mL). The mixture was stirred at 60 °C until completion, as judged by disappearance of starting material in TLC. Solvent and excess HCl were then removed under vacuum, and the crude salt was washed with minimum amount of water to remove excess HCl and recrystallised from CH_2Cl_2 to furnish pure compounds (**3a-f**).

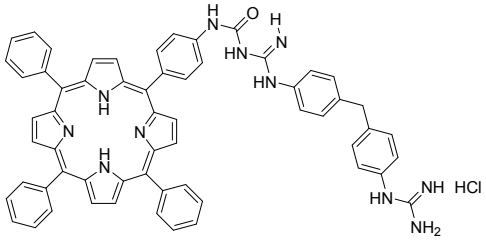

3a: Yield = 40 mg, 0.04 mmol, 55%. m.p. >300 °C. **UV–vis** (CH_3OH,: λ_{max} (ε) 416 (125,893), 513 (6310), 547 (3981), 592 (1995), 649 nm (2512 L mol^{-1} cm^{-1}). **IR** (ATR), ν_{max} (cm^{-1}): 3362, 1719, 1680, 1629, 1482, 1185. **^{1}H NMR** (400 MHz, MeOD): δ. 8.83-8.78 (m, 8H), 8.60 (s, 8H), 8.27 (s, 2H), 8.07 (s, 9H), 7.47 (d, *J* = 7.7 Hz, 2H), 7.42-7.38 (m, 4H), 7.24 (d, *J* = 7.9 Hz, 2H), 4.11 ppm (s, 2H). **^{13}C NMR** (100 MHz, MeOD): δ. 157.0, 154.6, 151.9, 145.8, 145.7, 142.4, 140.8, 140.5, 140.4, 139.8, 139.78, 139.74, 139.6, 139.5, 138.7, 138.6, 136.2, 133.2, 132.5, 131.4, 130.9, 130.6, 130.5, 128.9, 128.6, 128.2, 126.7, 125.8, 125.7, 122.9, 122.6, 119.7, 40.7 ppm. **HRMS** (ESI): *m/z* Calcd. for $C_{60}H_{48}N_{11}O$ $(M+H)^+$: 938.4043, Found: 938.4041.

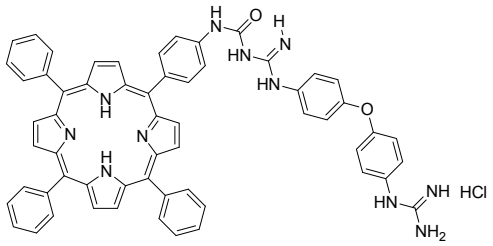

3b: Yield = 55 mg, 0.056 mmol, 68%. m.p. >300 °C. **UV–vis** (CH_3OH): λ_{max} (ε) 430 (79,433), 521 (10,000), 558 (6310), 596 (3981), 653 nm (3162 L mol^{-1} cm^{-1}). **IR** (ATR), ν_{max} (cm^{-1}): 3340, 1725, 1674, 1629, 1583, 1492. **^{1}H NMR** (400 MHz, MeOD): δ. 8.87 (s, 8H), 8.62 (s, 7H), 8.28 (s, 2H), 8.06 (s, 9H), 7.50 (d, *J* = 8.3 Hz, 2H), 7.34 (d, *J* = 8.6 Hz, 3H), 7.25- 7.20 ppm (m, 4H). **^{13}C NMR** (100 MHz, MeOD): δ. 157.5, 157.0, 156.1, 154.5, 151.5, 145.5, 145.47, 145.44, 139.3, 138.57, 138.55, 138.52, 138.50, 138.4, 130.35, 130.34, 130.29, 128.6, 128.3, 128.1, 127.79, 127.72, 127.68, 122.8, 122.3, 120.3, 120.2, 120.1, 199.9 ppm. **HRMS** (ESI): *m/z* Calcd. for $C_{59}H_{46}N_{11}O_2$ $(M+H)^+$: 940.3836, Found: 940.3818.

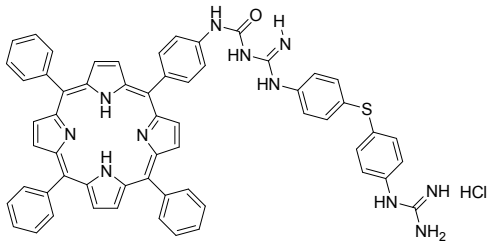

3c: Yield = 45 mg, 0.045 mmol, 55%. m.p. >300 °C. **UV–vis** (CH_3OH): λ_{max} (ε) 429 (100,000), 519 (15,849), 557 (10,000), 591 (7943), 650 nm (6310 L mol^{-1} cm^{-1}). **IR** (ATR), ν_{max} (cm^{-1}): 3311, 1731, 1680, 1487. **^{1}H NMR** (400 MHz, MeOD): δ. 8.83 (s, 9H), 8.63 (s, 6H), 8.30 (s, 2H), 8.07 (s, 9H), 7.94-7.87 (m, 1H), 7.54-7.48 (s, 6H), 7.32 ppm (s, 2H). **^{13}C NMR** (100 MHz, MeOD): δ. 156.6, 154.3, 151.4, 146.4, 146.3, 146.06, 146.04, 145.97, 145.94, 145.90, 139.54, 139.51, 138.4, 138.3, 137.0, 134.6, 133.6, 133.1, 132.8, 132.3, 132.0, 131.7, 130.2, 129.6, 129.5, 129.4, 128.4, 127.2, 126.6, 126.0, 125.9, 125.3, 122.9, 122.5,

119.46, 119.45 ppm. **HRMS** (ESI): *m/z* Calcd. for $C_{59}H_{46}N_{11}OS$ $(M+H)^+$: 956.3608, Found: 956.3597.

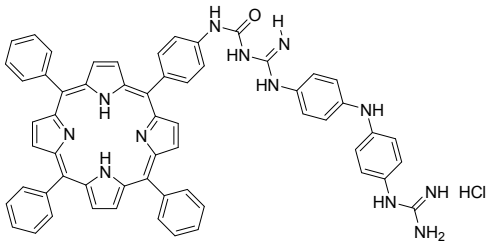

3d: Yield = 22 mg, 0.022 mmol, 45%. m.p. >300 °C. **UV–vis** (CH_3OH): λ_{max} (ε) 425 (79,433), 520 (7943), 552 (3981), 591 (3162), 648 nm (2512 L mol^{-1} cm^{-1}). **IR** (ATR), ν_{max} (cm^{-1}): 3226, 1612, 1490, 1289. **^{1}H NMR** (400 MHz, MeOD): δ. 8.75 (s, 9H), 8.57 (s, 5H), 8.29 (s, 3H), 8.04 (s, 7H), 7.29-7.14 ppm (m, 11H). **^{13}C NMR** (100 MHz, MeOD): δ. 157.4, 154.9, 151.9, 146.1, 146.0, 145.9, 145.8, 144.7, 143.6, 143.2, 139.7, 138.69, 138.68, 136.1, 135.94, 135.93, 130.6, 130.0, 129.72, 129.70, 129.59, 129.58, 129.46, 129.43, 128.8, 128.2, 128.1, 127.8, 127.54, 127.51, 127.1, 126.6, 124.6, 123.9, 123.2, 122.85, 122.81, 119.7, 118.8, 118.7, 118.2, 118.1, 117.9 ppm. **HRMS** (ESI): *m/z* Calcd. for $C_{59}H_{47}N_{12}O$ $(M+H)^+$: 939.3996, Found: 939.3988.

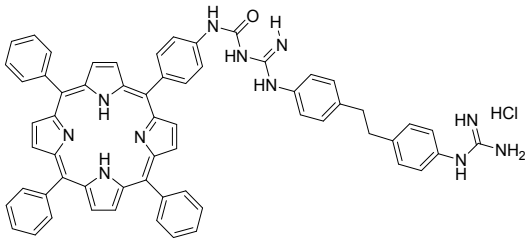

3e: Yield = 25 mg, 0.025 mmol, 61%. m.p. >300 °C. **UV–vis** (CH_3OH): λ_{max} (ε) 417 (125,893), 523 (15,849), 557 (10,000), 591 (5012), 648 nm (6310 L mol^{-1} cm^{-1}). **IR** (ATR), ν_{max} (cm^{-1}): 3328, 1731, 1674, 1485, 1295. **^{1}H NMR** (400 MHz, MeOD): δ. 8.76 (s, 9H), 8.57 (s, 7H), 8.27 (s, 2H), 8.05 (s, 9H), 7.45- 7.36 (m, 6H), 7.19 (d, *J* = 6.7 Hz, 2H), 3.03 ppm (s, 4H). **^{13}C NMR** (100 MHz, MeOD): δ. 156.7, 154.3, 141.5, 145.9, 145.88, 145.85, 145.83, 145.81, 145.7, 145.65, 145.62, 145.59, 145.56, 142.7, 141.3, 139.4, 138.33, 138.31, 138.29, 138.24, 135.6, 132.5, 130.8, 130.2, 129.8, 129.4, 129.3, 129.26, 129.22, 129.17. 129.14. 128.5, 126.2, 125.3, 122.7, 122.3, 119.4 ppm. **HRMS** (ESI): *m/z* Calcd. for $C_{61}H_{49}N_{11}O$ $(M+H)^+$: 951.4122, Found: 951.4161.

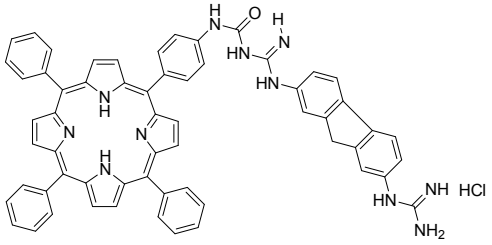

3f: Yield = 32 mg, 0.032 mmol, 70%. m.p. >300 °C. **UV–vis** (CH_3OH): λ_{max} (ε) 417 (79,433), 514 (10,000), 549 (5012), 590 (3981), 625 nm (3162 L mol^{-1} cm^{-1}). **IR** (ATR), ν_{max} (cm^{-1}): 3306, 1668, 1583, 1487, 1221. **^{1}H NMR** (400 MHz, MeOD): δ. 8.79 (s, 9H), 8.60 (d, *J* = 4.4

Hz, 8H), 8.28 (d, *J* = 7.5 Hz, 2H), 8.06 (s, 10H), 7.73 (s, 1H), 7.57 (s, 1H), 7.52 (d, *J* = 7.8 Hz, 1H), 7.35 (d, *J* = 7.9 Hz, 1H), 4.11 ppm (s, 2H). **^{13}C NMR** (100 MHz, MeOD): δ. 157.1, 154.8, 151.9, 146.1, 145.9, 141.7, 140.4, 140.2, 139.8, 139.78, 139.71, 139.6, 138.7, 138.67, 138.64, 138.62, 138.5, 135.9, 134.3, 132.1, 130.7, 130.6, 129.7, 129.5, 129.47, 129.41, 128.8, 125.6, 124.6, 123.5, 123.2, 122.8, 122.5, 121.8, 121.7, 121.4, 119.6, 36.9 ppm. **HRMS** (ESI): *m/z* Calcd. for $C_{60}H_{46}N_{11}O$ $(M+H)^+$: 936.3887, Found: 936.3876.

*General procedure for porphyrin metallation (**4a** and **4e**)*

Metallation of porphyrins was achieved by stirring porphyrins (**3a** and **3e,** 0.05 mmol) and zinc(II)acetate dihydrate (0.4 mmol) in 3:1 dichloromethane/methanol. The solution was stirred overnight at room temperature under nitrogen atmosphere. The solvent was evaporated under vacuum and obtained residues were washed with minimum water (2 × 5 mL) to remove excess of $Zn(OAc)_2$ followed by recrystallisation from DCM to furnish the pure compounds as acetate salts.

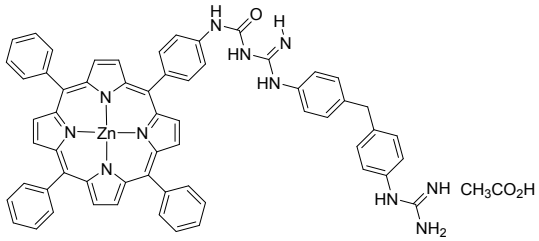

4a: Yield = 17 mg, 0.016 mmol, 50%. m.p. >300 °C. **UV–vis** (CH_3OH): λ_{max} (ε) 420 (100,000), 555 (7943), 598 nm (2512 L mol^{-1} cm^{-1}). **IR** (ATR), ν_{max} (cm^{-1}): 3311, 1731, 1668, 1583, 1532, 1306. **^{1}H NMR** (400 MHz, MeOD): δ. 8.90 (s, 1H), 8.89 (s, 1H), 8.82-8.80 (m, 6H), 8.18 (d, *J* = 6.7 Hz, 7H), 8.07 (d, *J* = 8.0 Hz, 2H), 7.86 (d, *J* = 7.9 Hz, 2H), 7.75- 7.73 (m, 10H), 7.36 (d, *J* = 8.0 Hz, 2H), 7.21-7.09 (m, 4H), 3.92 ppm (s, 2H). **^{13}C NMR** (100 MHz, MeOD): δ.150.2, 150.0, 143.5, 141.3, 134.5, 134.2, 131.9, 131.0, 130.0, 129.3, 126.9, 126.0, 125.3, 123.1, 120.3, 40.2 ppm. **HRMS** (ESI): *m/z* Calcd. for $C_{60}H_{45}N_{11}OZn$ $(M)^+$: 999.3100, Found: 999.3072.

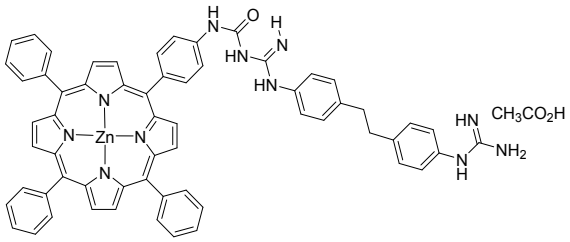

4e: Yield = 22 mg, 0.020 mmol, 45%. m.p. >300 °C. **UV–vis** (CH_3OH): λ_{max} (ε): 423 (100,000), 558 (6310), 598 nm (1995 L mol^{-1} cm^{-1}). **IR** (ATR), ν_{max} (cm^{-1}): 3345, 1735, 1668, 1515, 1323. **^{1}H NMR** (400 MHz, MeOD): δ. 8.90 (s, 1H), 8.89 (s, 1H), 8.82-8.81 (m, 6H), 8.18 (s, 7H), 8.08 (d, *J* = 8.3 Hz, 2H), 7.87 (d, *J* = 4 Hz, 2H), 7.75- 7.73 (m, 10H), 7.33 (d, *J* = 7.3 Hz, 2H), 7.20 (d, *J* = 8.4 Hz, 4H), 2.82 ppm (s, 4H). **^{13}C NMR** (100 MHz, MeOD): δ.148.7, 148.5, 148.4, 142.0, 139.8, 133.0, 132.6, 129.6, 129.5, 128.3, 128.2, 128.1, 127.5,

125.4, 124.5, 123.7, 123.6, 123.5, 121.9, 118.8, 118.7, 35.2, 35.1 ppm. **HRMS** (ESI): *m/z* Calcd. for $C_{61}H_{47}N_{11}OZn$ $(M)^+$: 1013.3257, Found: 1013.3263.

Biophysical studies

Oligonucleotides

All oligonucleotides (Table S1) were purchased from Eurogentec (Belgium) and used without further purification for thermal melting, CD and UV-Vis titration experiments. The concentrations of oligonucleotides were determined using appropriate molar extinction coefficient values ε (λ = 260 nm). The salmon sperm DNA was purchased from Sigma Aldrich (extinction coefficient ε_{260} = 6600 cm^{-1} M^{-1} base). The oligonucleotides were pre-folded in their respective buffers by heating at 90 °C for five minutes and gradually cooled to room temperature and stored at -20 °C prior to performing experiments.

Table S1.- Oligonucleotides used for UV thermal melting assays and titration studies.

Oligonucleotide	Origin	Sequence (5'-3')	
24TTA	Human telomeric sequence	TAGGGTTAGGGTTAGGGTTAGGGT	G4 Hybrid
22AG	Human telomeric sequence 2	AGGGTTAGGGTTAGGGTTAGGG	G4 Antiparallel
c-MYC	c-Myc promoter sequence	TGAGGGTGGGTAGGGTGGGTAA	G4 Parallel
c-KIT2	c-Kit promoter sequence 2	CGGGCGGGCGCGAGGGAGGGG	G4 Parallel
c-KIT1	c-Kit promoter sequence 1	AGGGAGGGCGCTGGGAGGAGGG	G4 Parallel
ds12	Double helix model	CGCGAATTCGCG	Deoxyoligo nucleotide

UV-Thermal Melting Experiments

Thermal melting experiments were conducted with a Varian Cary 300 Bio spectrophotometer equipped with a 6 × 6 multicell temperature-controlled block. Temperature was monitored with a thermistor inserted into a 1 mL quartz cuvette containing the same volume of buffer as in the sample cells. Absorbance changes at 295 nm and 260 nm for G4 DNA and ssDNA respectively, were monitored from a range of 30 °C to 90 °C with a heating rate of 1 °C/ min and a data collection rate of five points per °C. The stock solution of G4s were prepared in 10 mM lithium cacodylate containing 100 mM of sodium chloride (for *24TTA* and *22AG*), 5 mM potassium phosphate buffer containing 20 mM KCl (for *c-MYC* and *c-KIT2*) and 10 mM potassium phosphate containing 100 mM KCl (for the rest). The stock solution of *st-DNA* was

prepared in phosphate buffer solutions contained 10 mM Na_2HPO_4/NaH_2PO_4 adjusted to pH 7. The stock solution of ligands was prepared in EtOH (1 mM). A quartz cell with a 1-cm path length was filled with a 1 mL solution of G4s (5 μM) or G4−ligand complex (1:2). For thermal melting study against st-DNA, DNA polymer (150 μM base) and the compound solution (15 μM) were prepared in the phosphate buffer, adjusted to pH 7 so that a ligand to DNA base ratio of 0.1 was obtained.

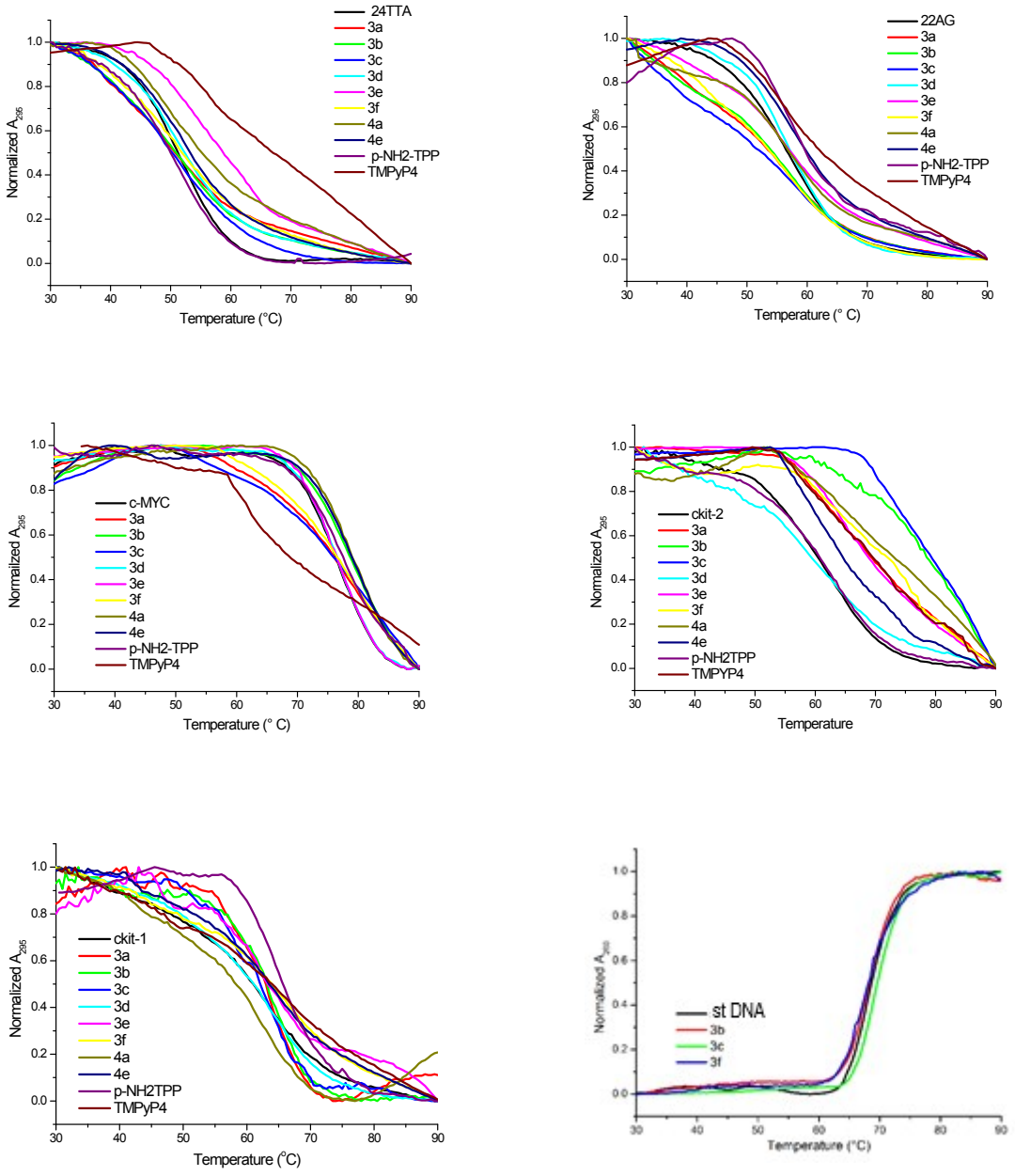

Figure S1. UV-thermal melting profiles of the examined G4-DNA (DNA : Ligand = 1:2) and st-DNA (ligand : DNA-base = 1:10) in the absence and presence of ligands.

FRET melting assays

FRET melting experiments were performed with dual-labelled oligonucleotides (see Table below). The oligonucleotides were pre-folded in 10 mM Lithium cacodylate buffer (pH 7.2) in the presence of 10 mM KCl and 90 mM LiCl, with a final oligonucleotide strand concentration of 0.2 μM. The ligand induced thermal stabilization ($\Delta T_{1/2}$) for every pre-folded oligonucleotide was determined by performing the difference between the temperature of mid-transition measured with and without the tested ligand. The ligands were added to a final concentration of 1 μM. FAM emission was recorded at 516 nm using 492 nm as the excitation wavelength as a function of temperature increasing from 25 °C to 95 °C at a rate of 1 °C/min. The experiment was done in 96-well microplate using a Stratagene Mx3005P real-time PCR device in duplicate conditions. The measured $\Delta T_{1/2}$ represents the average of two independent experiments. The selectivity of the ligands against duplexes was investigated by performed competition assays using the self-complementary ds26 duplex (5'-CAA TCG GAT CGA ATT CGA TCC GAT TG-3') as a duplex competitor both in the same buffer and in cacodylate containing 100 mM NaCl.

Table S2.- Dual-labelled oligonucleotides used for FRET melting assays

Oligonucleotide	Origin	Sequence (5'-3')	Structure type
F21T	Human telomeric DNA	FAM-$(GGGTTA)_3GGG$-TAMRA	Polymorphic
F21RT	Human telomeric RNA (TERRA)	FAM-$(GGGUUA)_3GGG$-TAMRA	Parallel
Fkit2T	c-Kit promoter sequence 2	FAM-$G_3CG_3CGCGAG_3AG_4$-TAMRA	Parallel
F21CTAT	Human telomeric DNA (mutant)	FAM-$(GGGCTA)_3GGG$-TAMRA	Antiparallel
FHiv32T	HIV PRO2 sequence	FAM-$CAG_3AG_2CGTG_2C_2TG_3CG_3A$-TAMRA	Polymorphic
FHiv321T	HIV PRO1 sequence	FAM-$T_2G_2C_2TG_3CG_3ACTG_3A$-TAMRA	Antiparallel
FdXT	Intramolecular duplex	FAM-TATAGCTATA-hexaethylene glycol-TATAGCTATA-TAMRA	Duplex

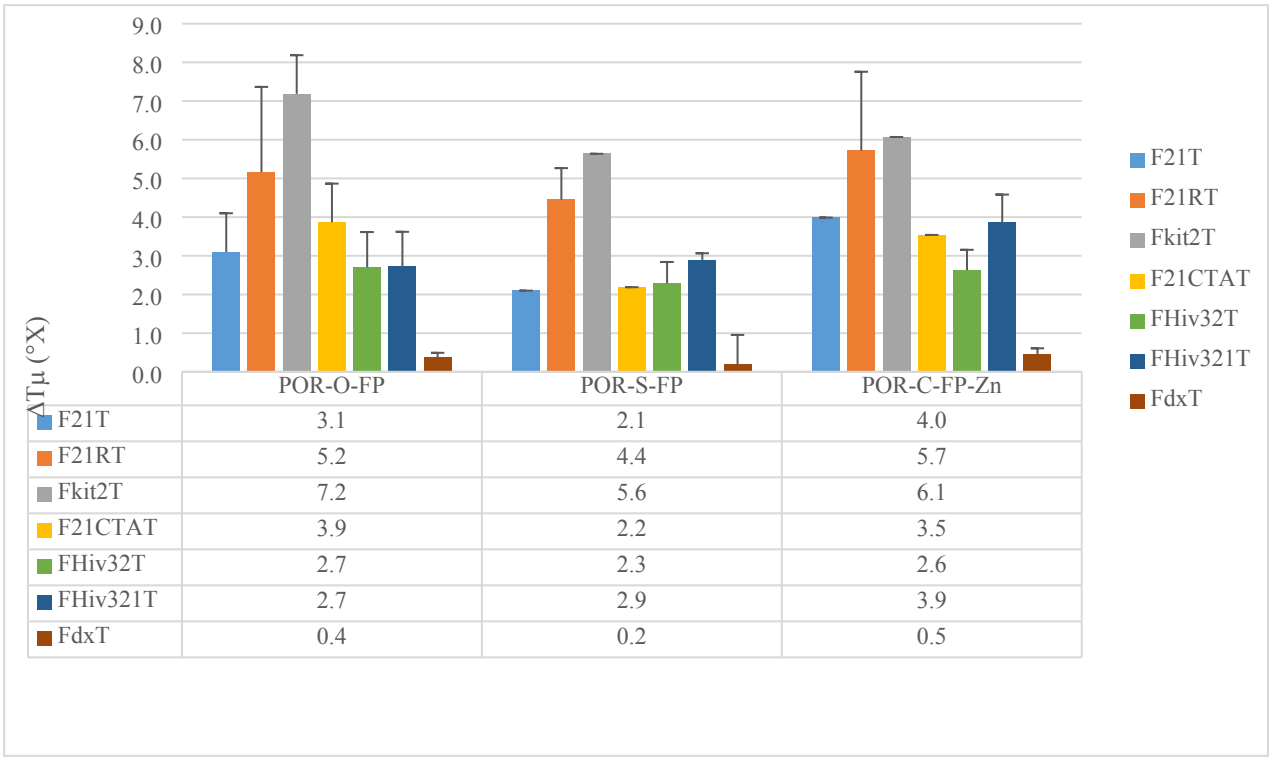

	POR-O-FP	POR-S-FP	POR-C-FP-Zn
F21T	3.1	2.1	4.0
F21RT	5.2	4.4	5.7
Fkit2T	7.2	5.6	6.1
F21CTAT	3.9	2.2	3.5
FHiv32T	2.7	2.3	2.6
FHiv321T	2.7	2.9	3.9
FdxT	0.4	0.2	0.5

Figure S2. FRET melting assay results. Thermal stabilization induced by the tested compounds (1 μM) on different G4 sequences (0.2 μM) in 10 mM lithium cacodylate pH 7.2 containing 10 mM KCl and 90 mM LiCl. These values represent the average of two experiments.

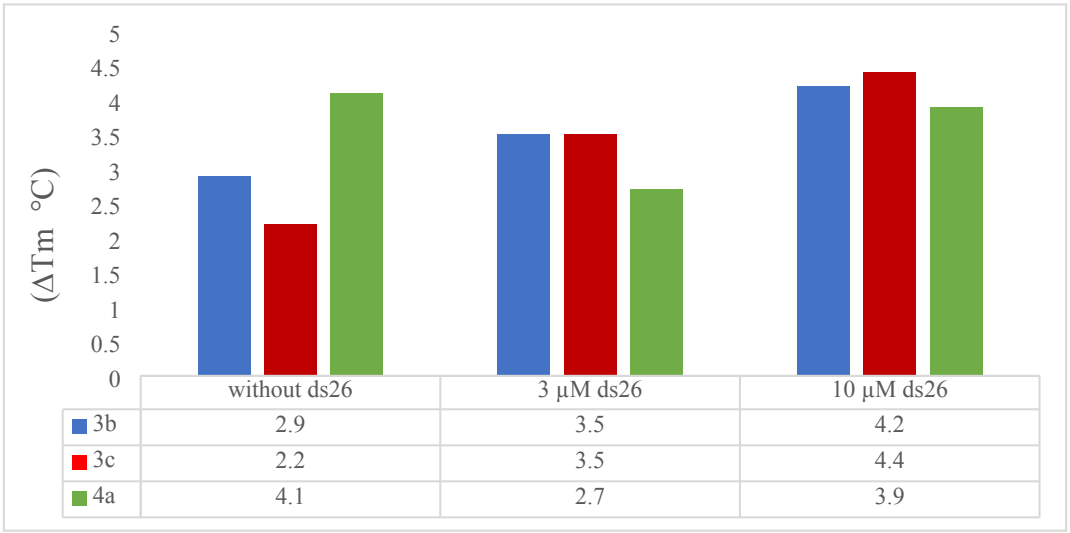

	without ds26	3 μM ds26	10 μM ds26
3b	2.9	3.5	4.2
3c	2.2	3.5	4.4
4a	4.1	2.7	3.9

Figure S3. FRET melting competition assay results. Thermal stabilization induced by the tested compounds (1 μM) on the F21T (0.2 μM) in 10 mM lithium cacodylate pH 7.2 containing 10 mM KCl and 90 mM LiCl, The duplex competitor (ds26) strand concentrations were 0, 3, and 10 μM. These values represent the average of two experiments.

Circular dichroism (CD) spectroscopy

CD-titrations for *c-KIT2* were recorded at 20 °C on a Jasco J-815 equipped with a Peltier temperature controller. Each spectrum corresponds to the average of four scans measured in 1-cm path-length quartz cells at 100 nm min^{-1} (bandwidth: 2 nm, data integration time: 1s). The oligonucleotide was pre-folded at 5 μM in 5 mM potassium phosphate buffer containing 20 mM KCl and stock solution of ligands were prepared in EtOH (1 mM). The CD spectrum was recorded using 1, 2 and 5 equivalents of ligands with incubation time of 10 min during each titration. All spectra were baseline subtracted and analysed using Origin 8.0 software.[4]

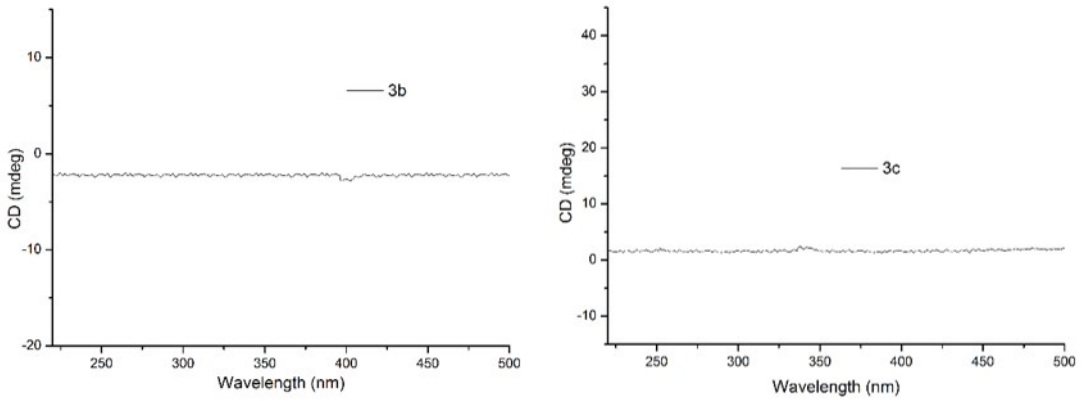

Figure S4. CD signature of ligands **3b** and **3c** (25 μM) in the absence of G4-DNA

UV-Vis titration studies

The UV-Vis titrations experiments were recorded on Specord 250 spectrophotometer in the 200–700 nm range at 25 °C with a 1 cm path-length quartz cell. The UV-Vis titrations were carried out by sequentially adding aliquots of each oligonucleotide (0 to 6 equivalents, pre-folded in 5 mM potassium phosphate buffer containing 20 mM KCl) to a UV-cell containing 3.0 µM solutions of **3b** or **3c** in 5 mM potassium phosphate buffer containing 20 mM KCl. All spectra recorded and results obtained are gathered in Figures S5-S16.

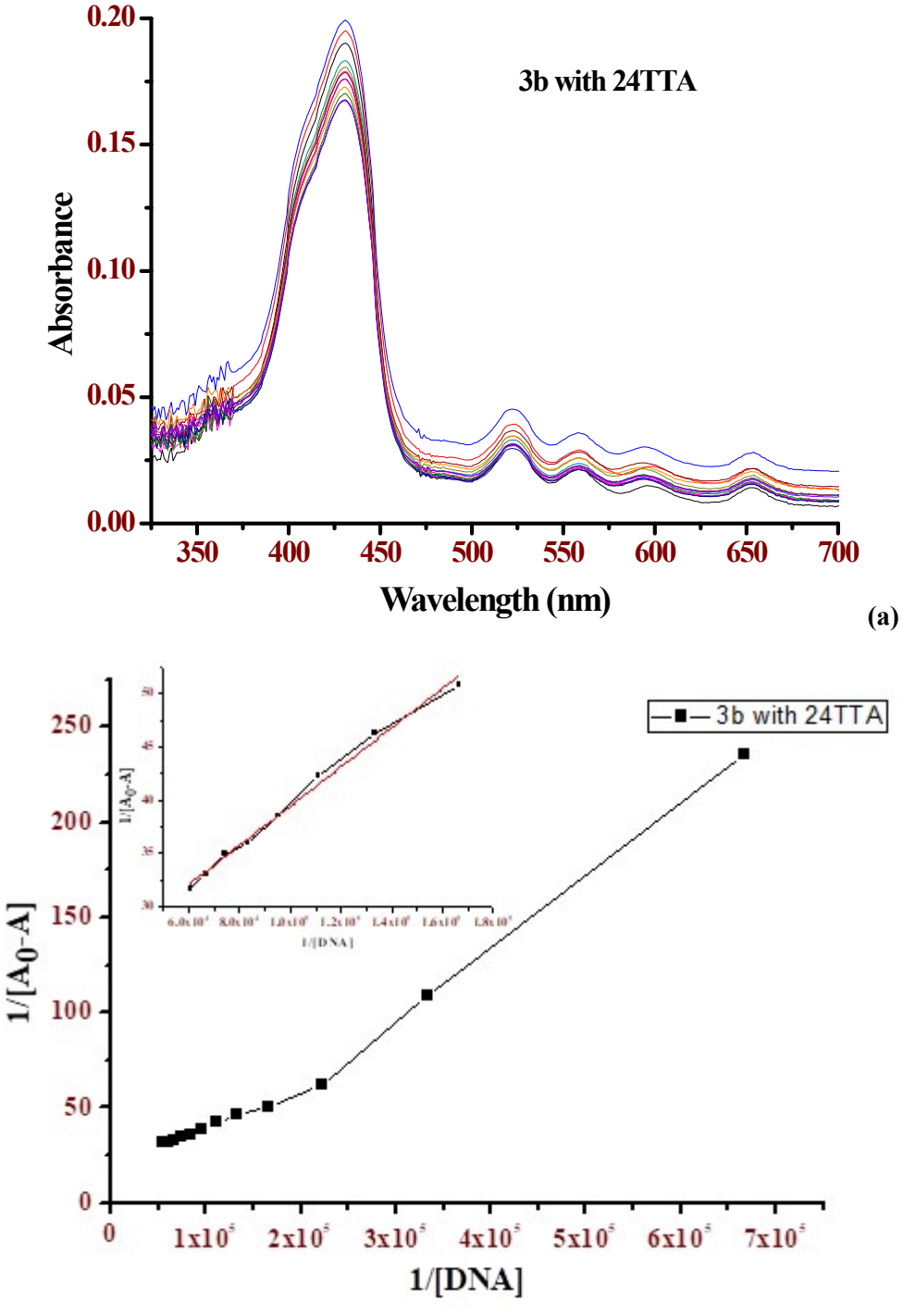

Figure S5. (**a**) UV-vis titrations of **3b** with 24TTA; **(b)** corresponding Benesi–Hildebrand plot (insert shows an enlargement of the initial points of the plot with 1/[DNA] between 0.6-1.8 10^5 M^{-1}, and the linear adjustment in red).

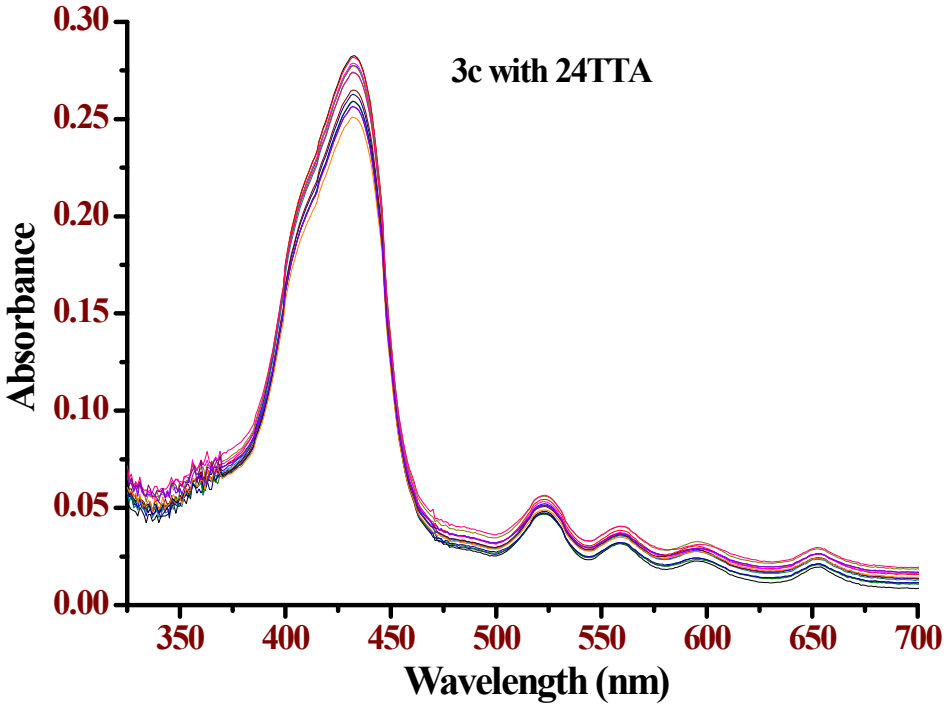

(a)

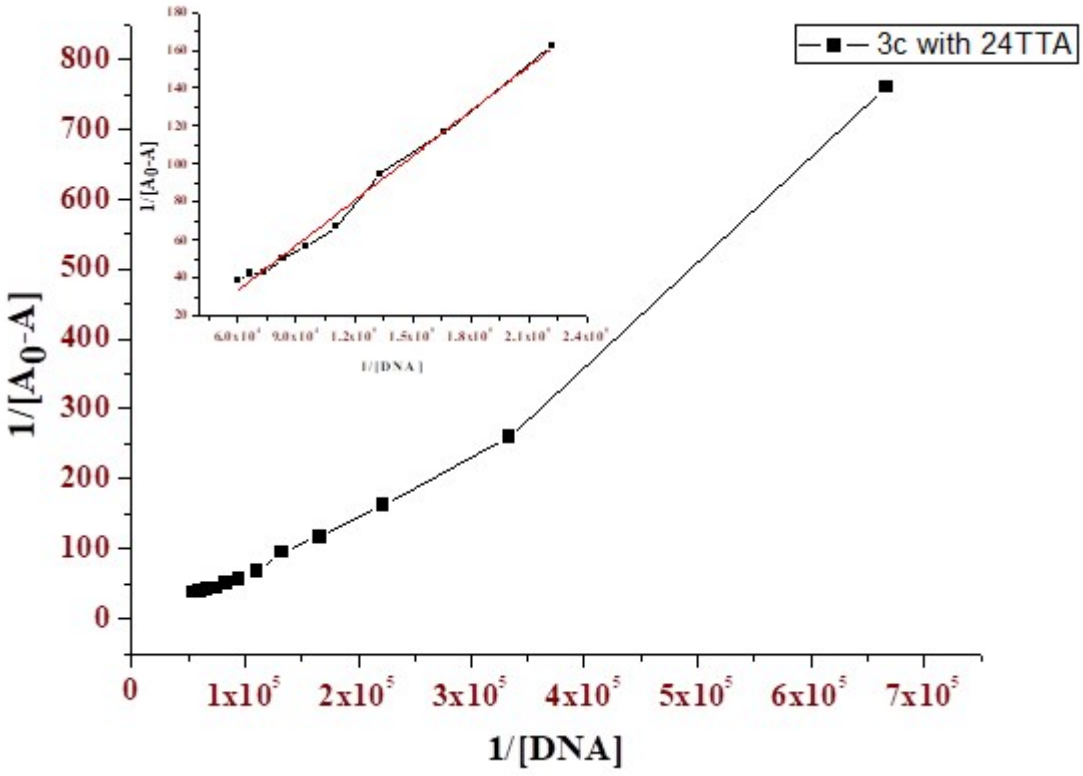

(b)

Figure S6. (a) UV-vis titrations of **3c** with 24TTA; **(b)** corresponding Benesi–Hildebrand plot (insert shows an enlargement of the initial points of the plot with 1/[DNA] between 0.6-2.4 10^5 M^{-1}, and the linear adjustment in red).

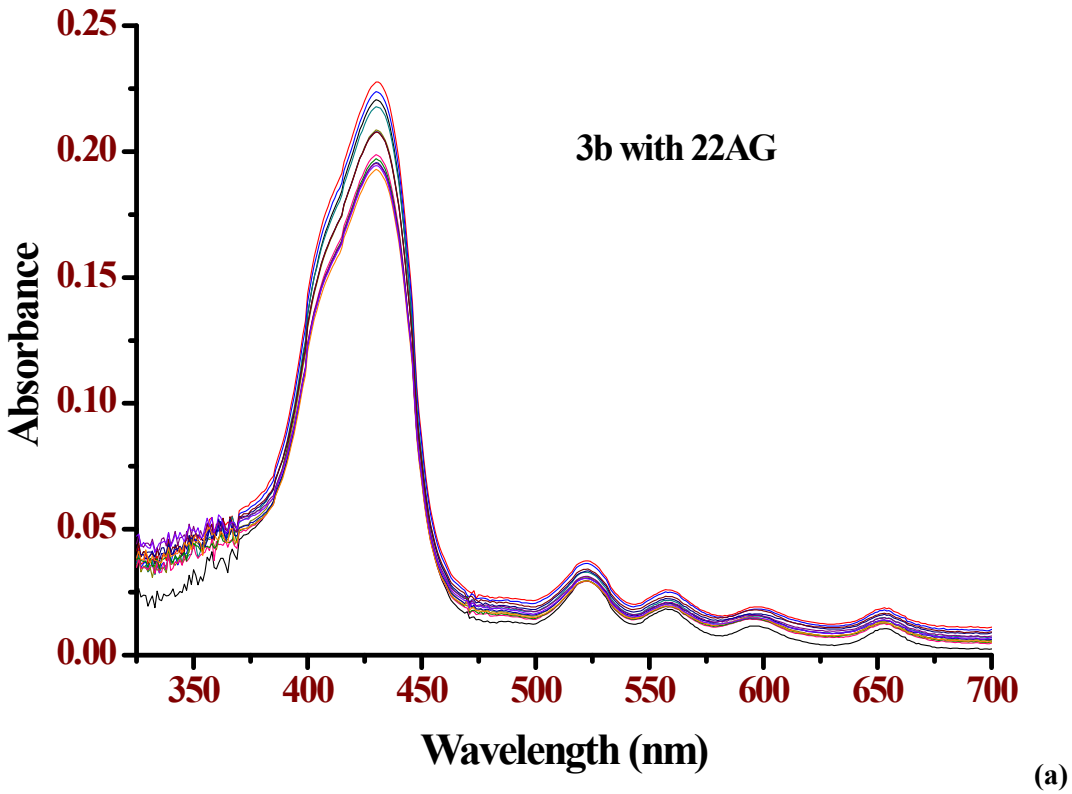

(a)

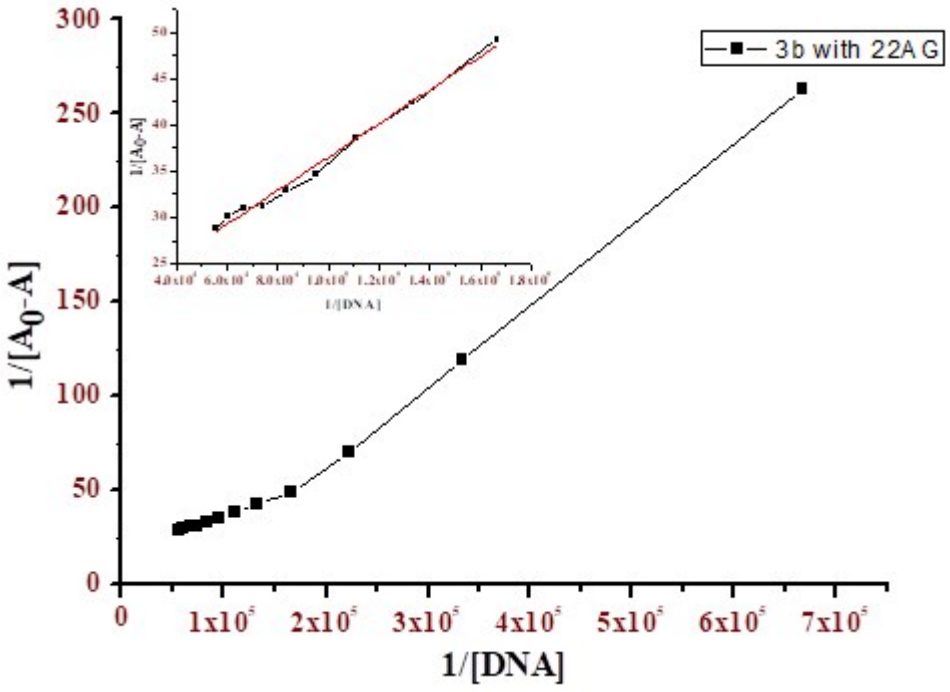

(b)

Figure S7. (a) UV-vis titrations of **3b** with 22AG. **(b)** corresponding Benesi–Hildebrand plot (insert shows an enlargement of the initial points of the plot with 1/[DNA] between 0.5-1.8 10^5 M^{-1}, and the linear adjustment in red).

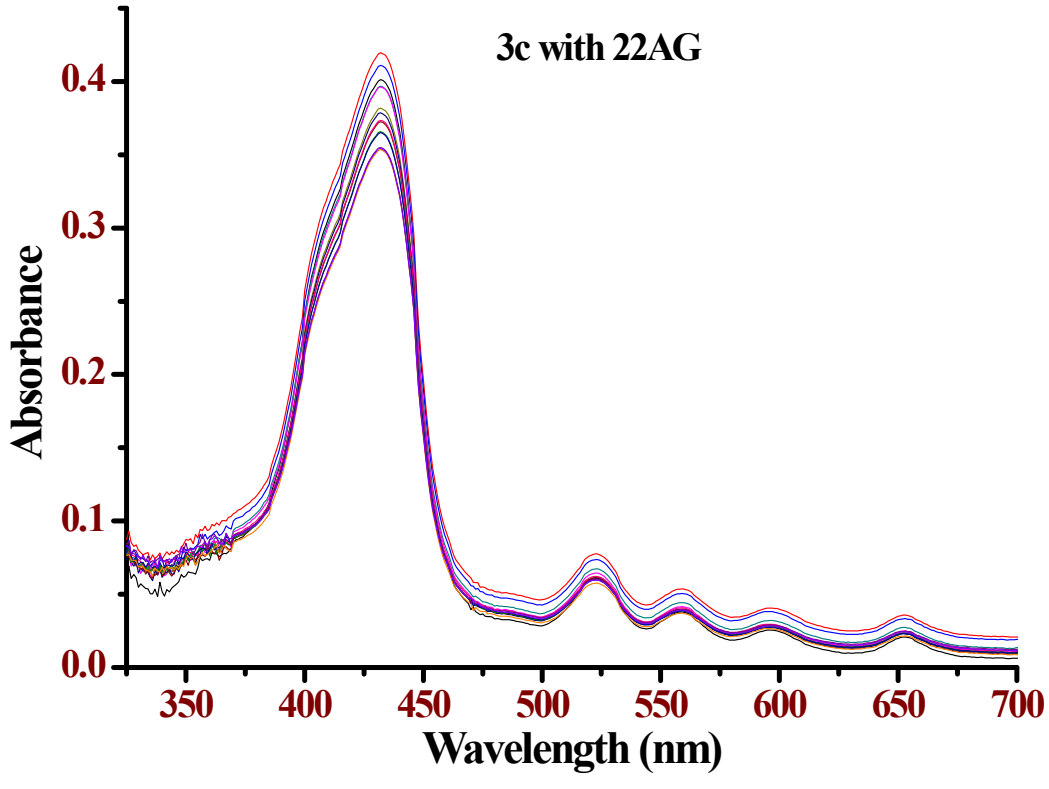

(a)

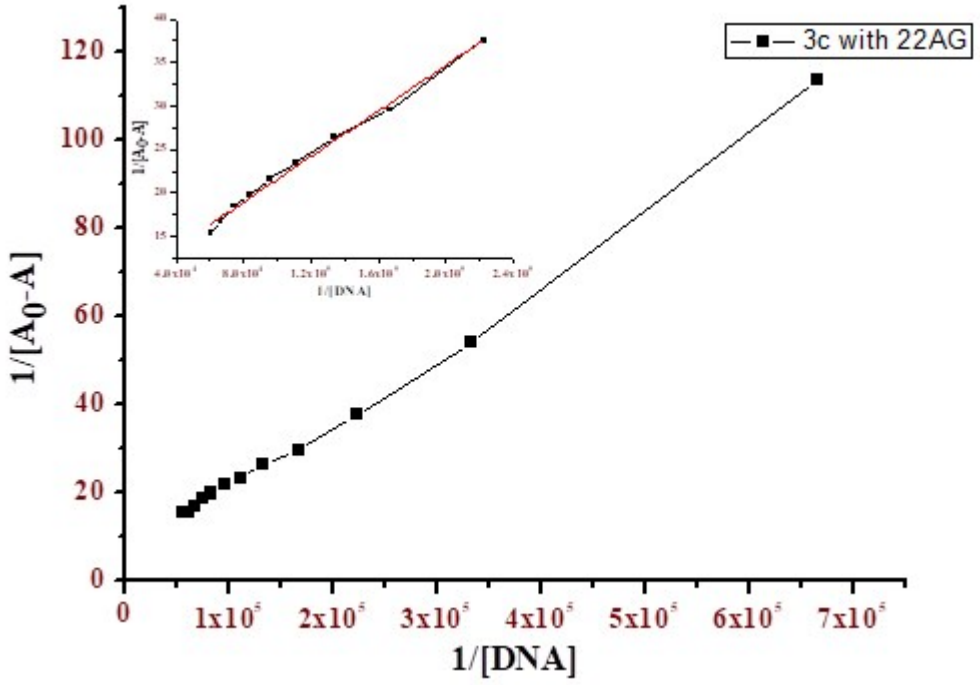

(b)

Figure S8. (a) UV-vis titrations of **3c** with 22AG. **(b)** corresponding Benesi–Hildebrand plot (insert shows an enlargement of the initial points of the plot with 1/[DNA] between 0.6-2.4 10^5 M^{-1}, and the linear adjustment in red).

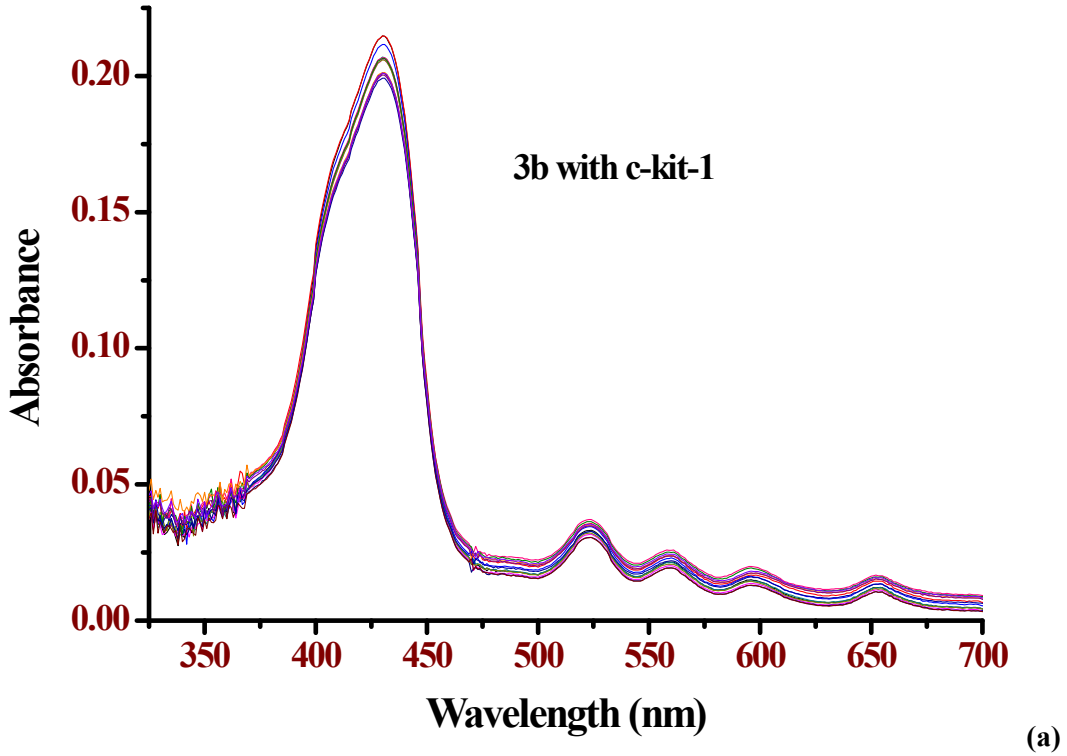

(a)

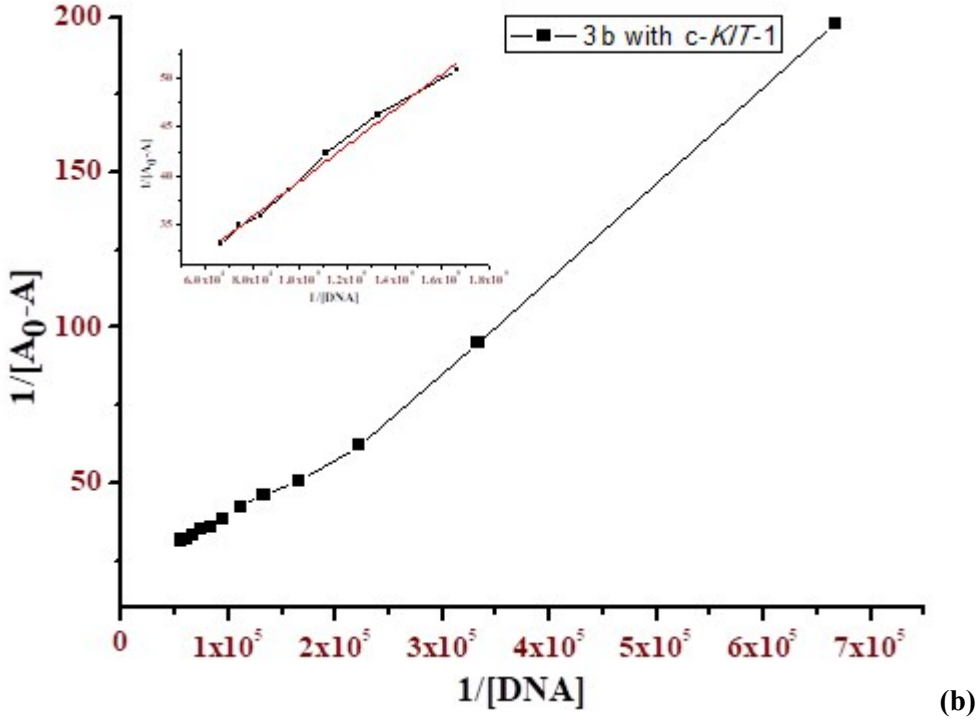

(b)

Figure S9. (a) UV-vis titrations of **3b** with c-kit-1; **(b)** corresponding Benesi–Hildebrand plot (insert shows an enlargement of the initial points of the plot with 1/[DNA] between 0.65-1.8 10^5 M^{-1}, and the linear adjustment in red).

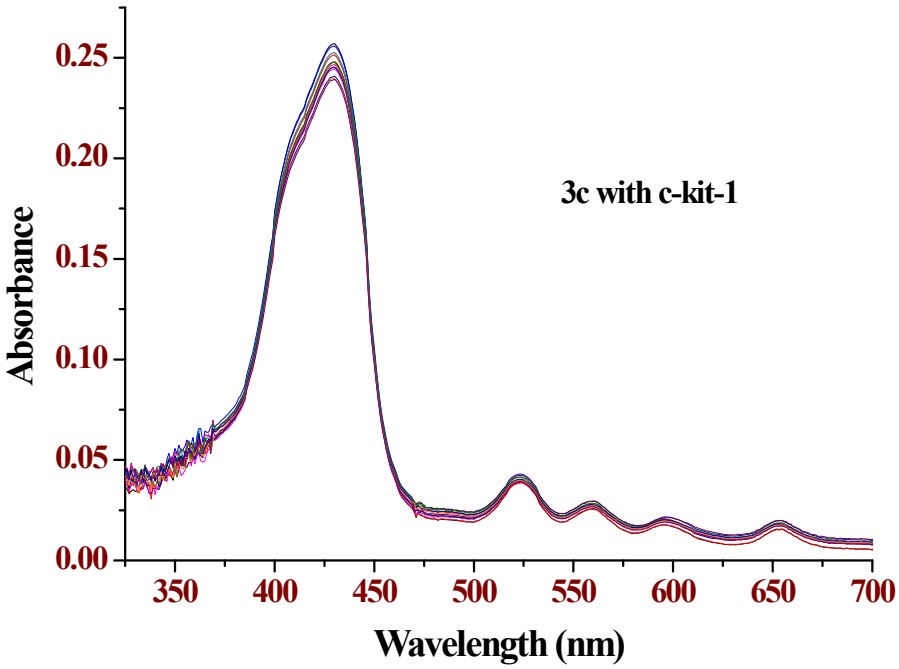

(a)

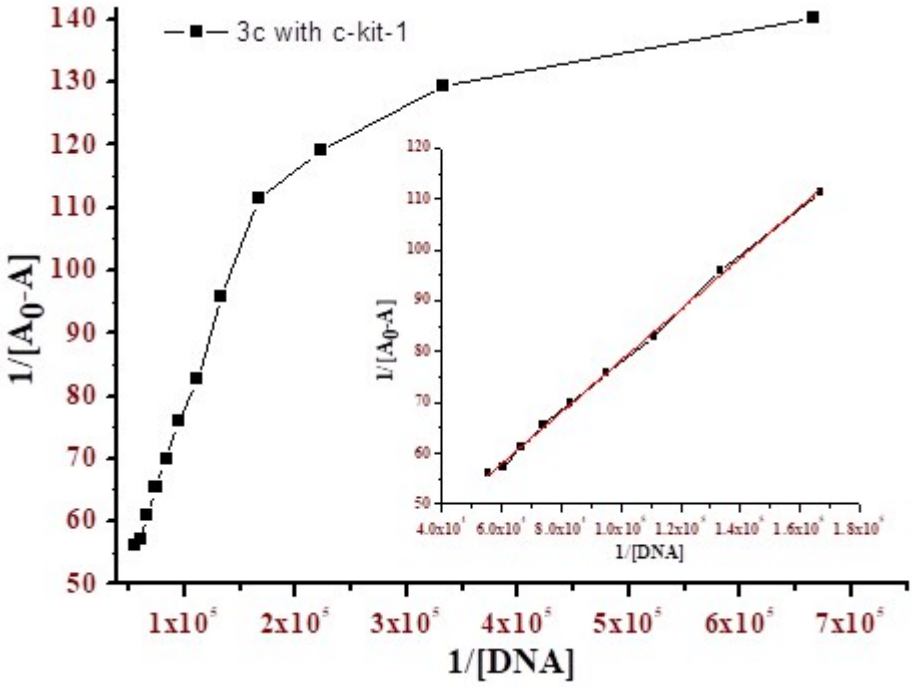

(b)

Figure S10. (a) UV-vis titrations of **3c** with c-kit-1; **(b)** corresponding Benesi–Hildebrand plot (insert shows an enlargement of the initial points of the plot with 1/[DNA] between 0.5-1.8 10^5 M^{-1}, and the linear adjustment in red).

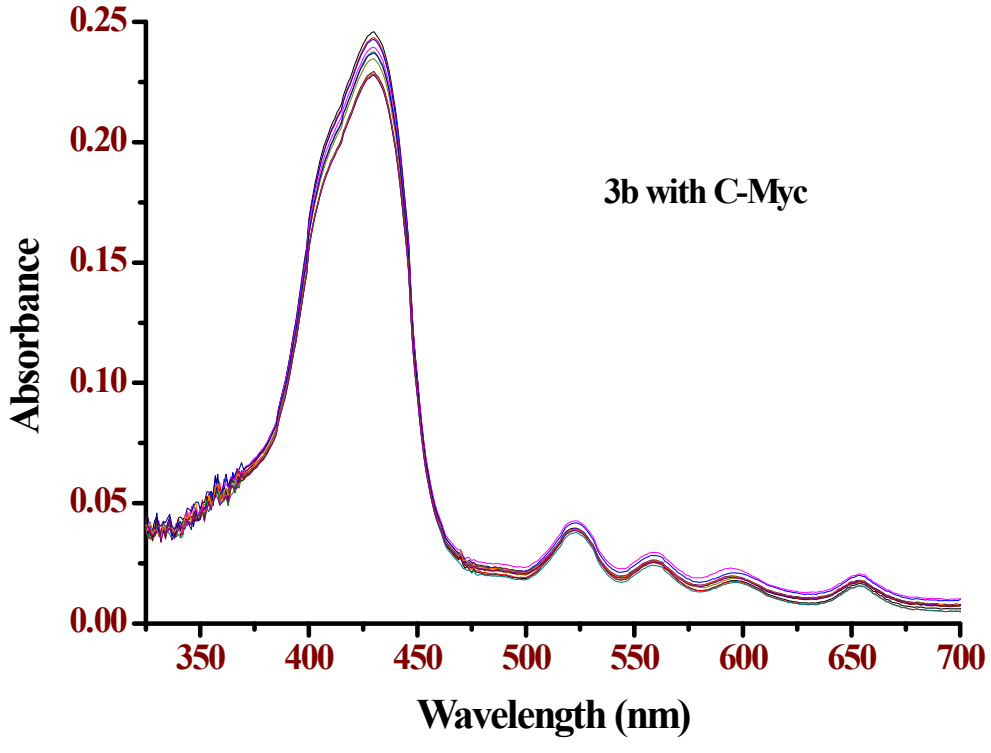

(a)

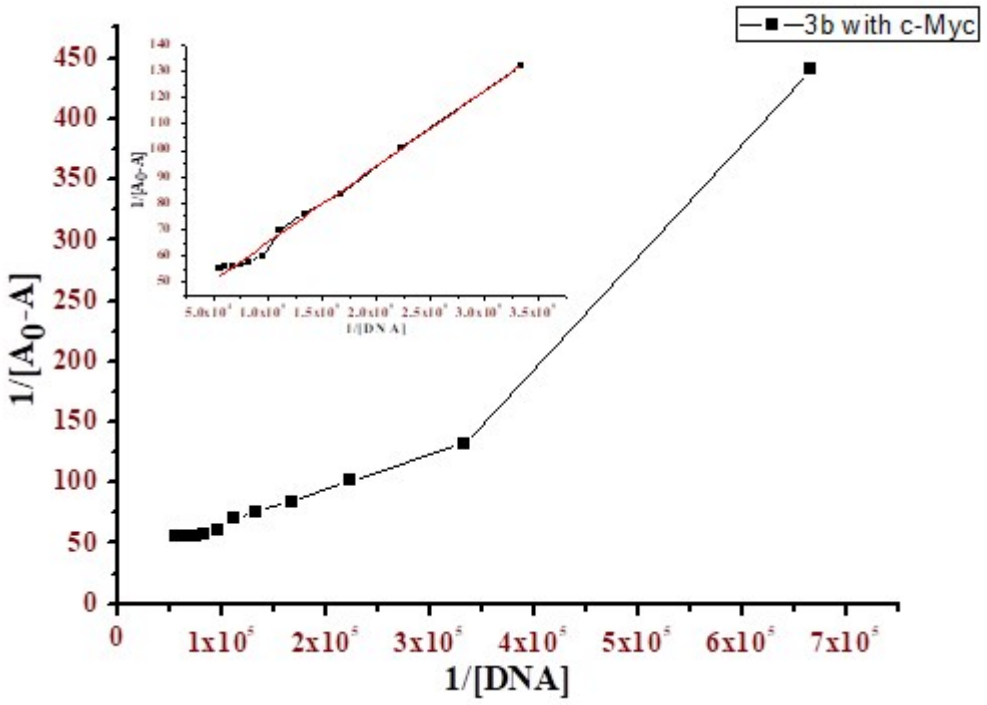

(b)

Figure S11. (a) UV-vis titrations of **3b** with c-Myc; **(b)** corresponding Benesi–Hildebrand plot (insert shows an enlargement of the initial points of the plot with 1/[DNA] between 0.5-3.5 10^5 M^{-1}, and the linear adjustment in red).

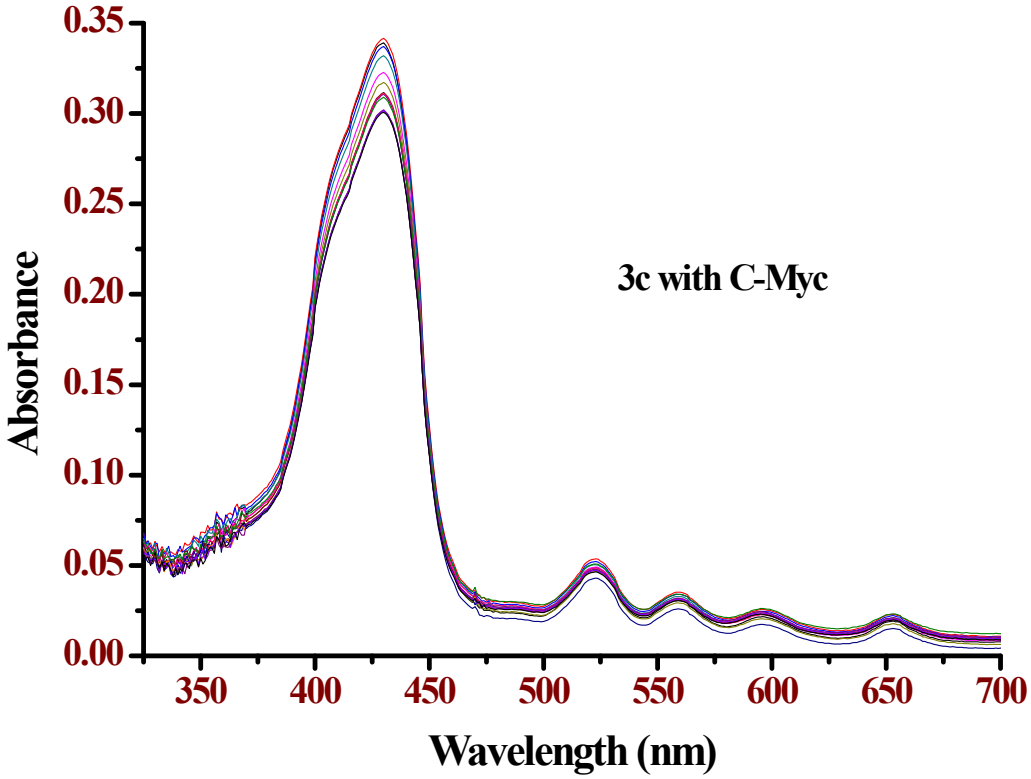

(a)

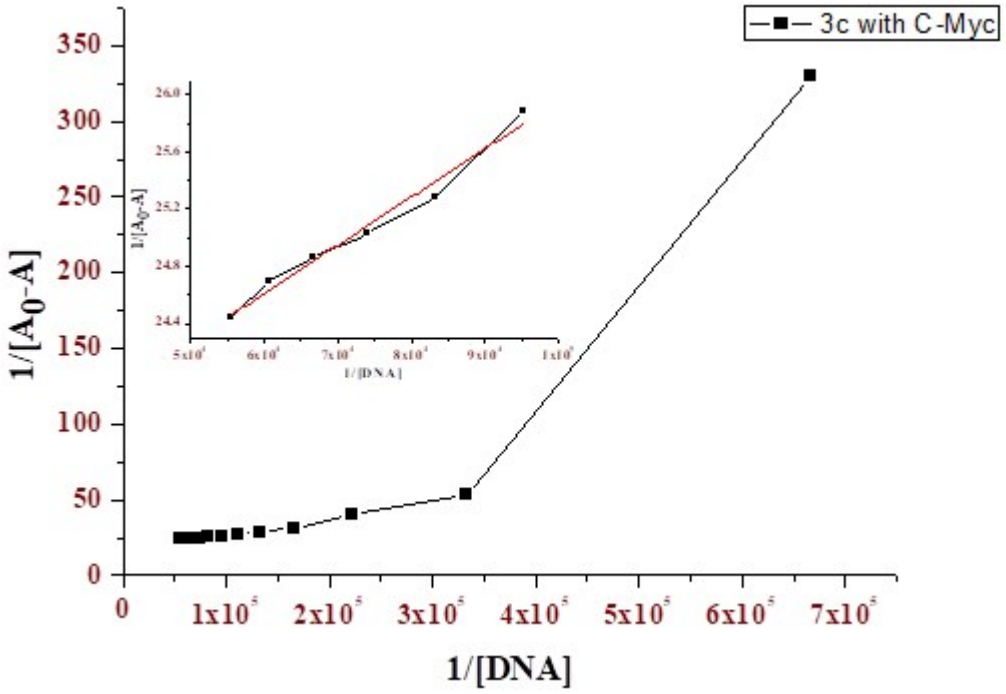

(b)

Figure S12. (a) UV-vis titrations of **3c** with c-Myc; **(b)** corresponding Benesi–Hildebrand plot (insert shows an enlargement of the initial points of the plot with 1/[DNA] between 0.55-1.0 10^5 M^{-1}, and the linear adjustment in red).

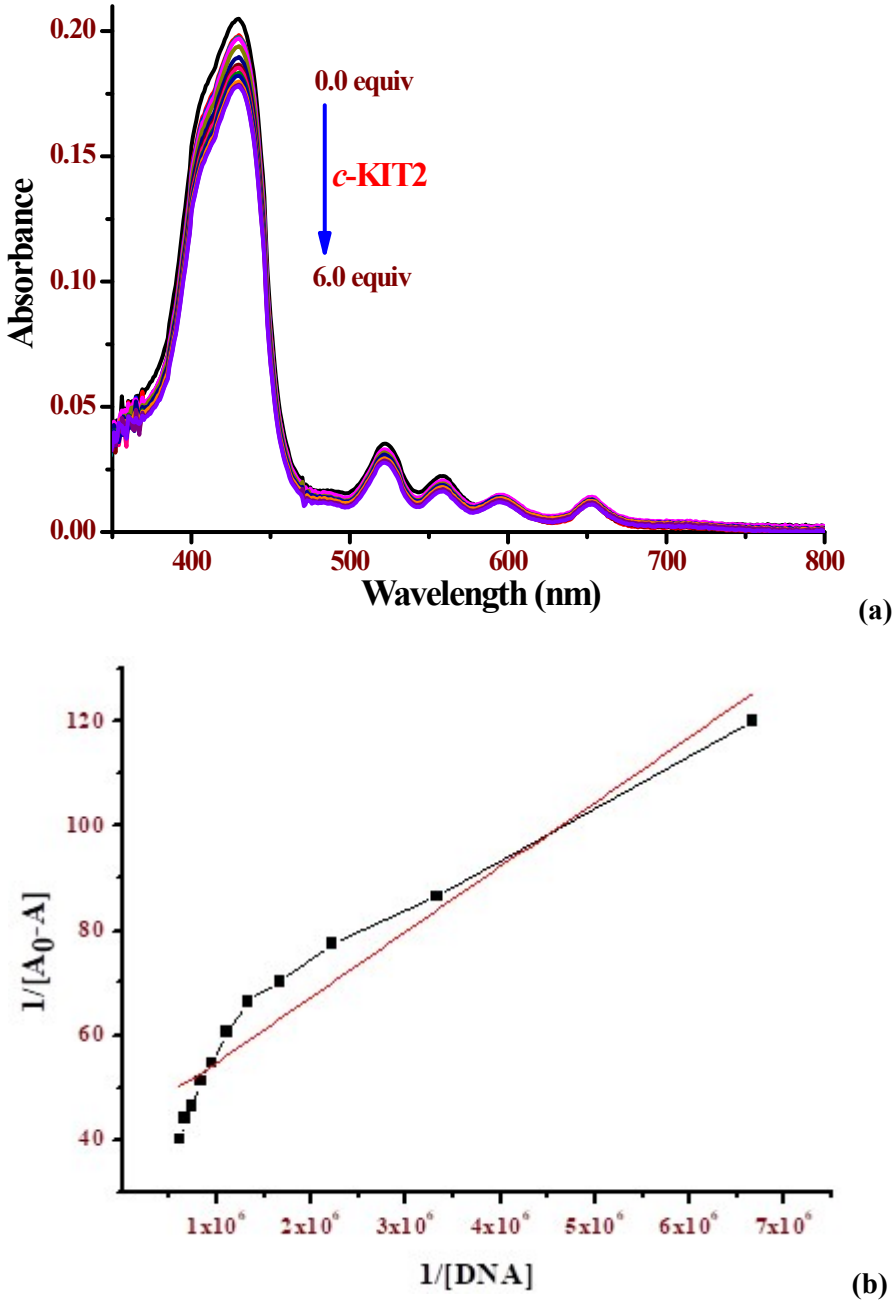

Figure S13. (a) UV-vis titrations of **3b** with c-Kit2; **(b)** corresponding Benesi–Hildebrand plot (linear adjustment in red).

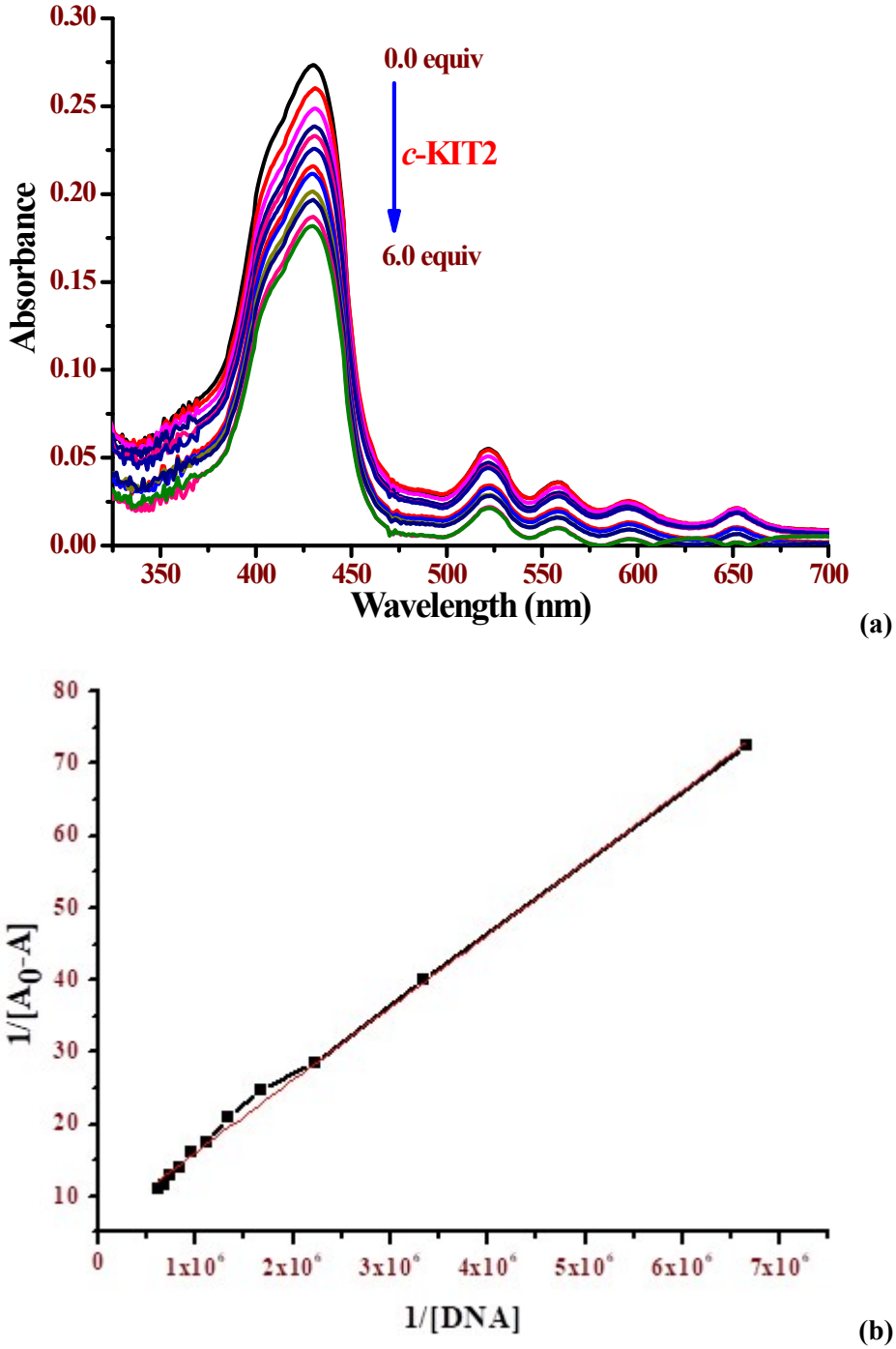

Figure S14. (a) UV-vis titrations of **3c** with c-Kit2; **(b)** corresponding Benesi–Hildebrand plot (linear adjustment in red).

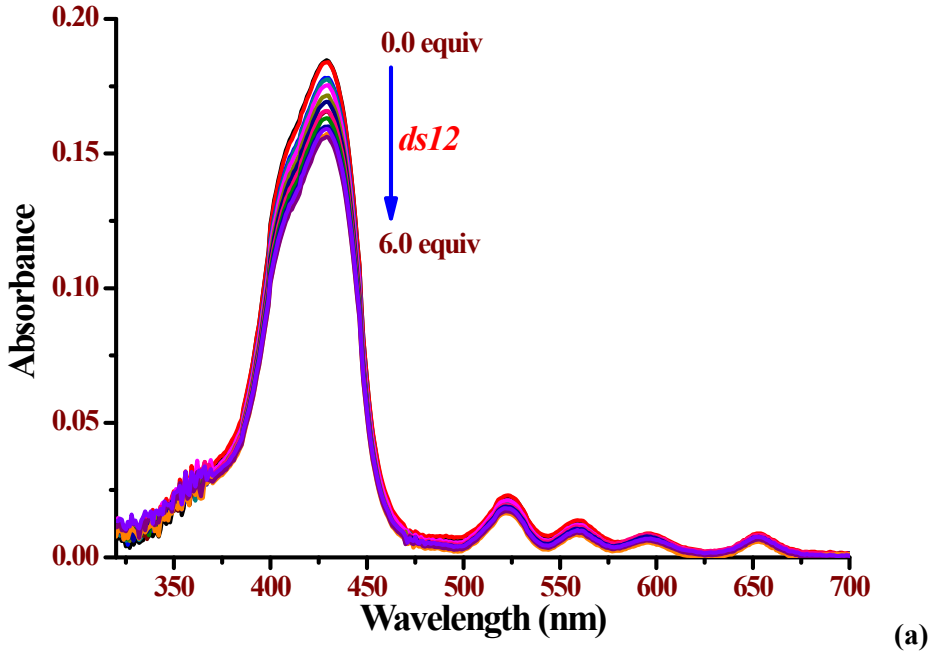

(a)

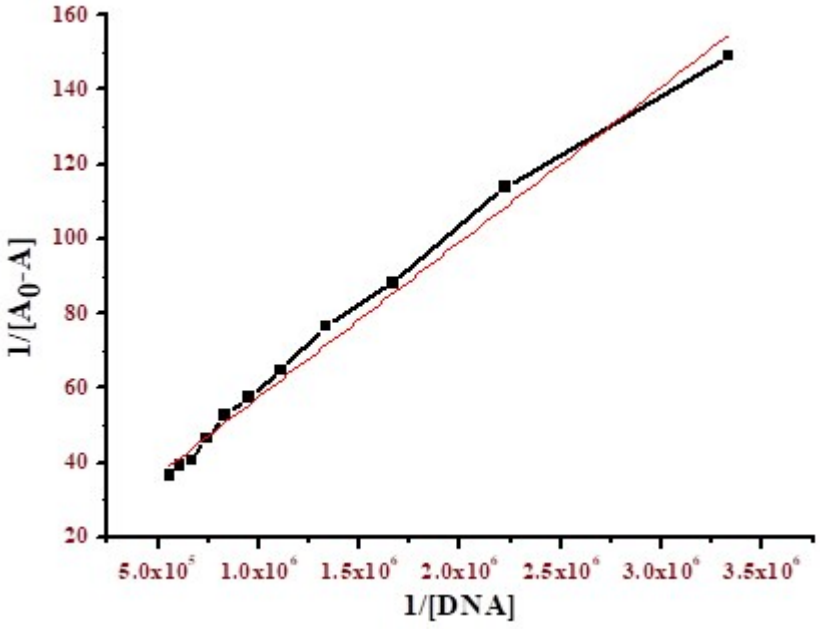

(b)

Figure S15. (a) UV-vis titrations of **3b** with ds12; **(b)** corresponding Benesi–Hildebrand plot (linear adjustment in red).

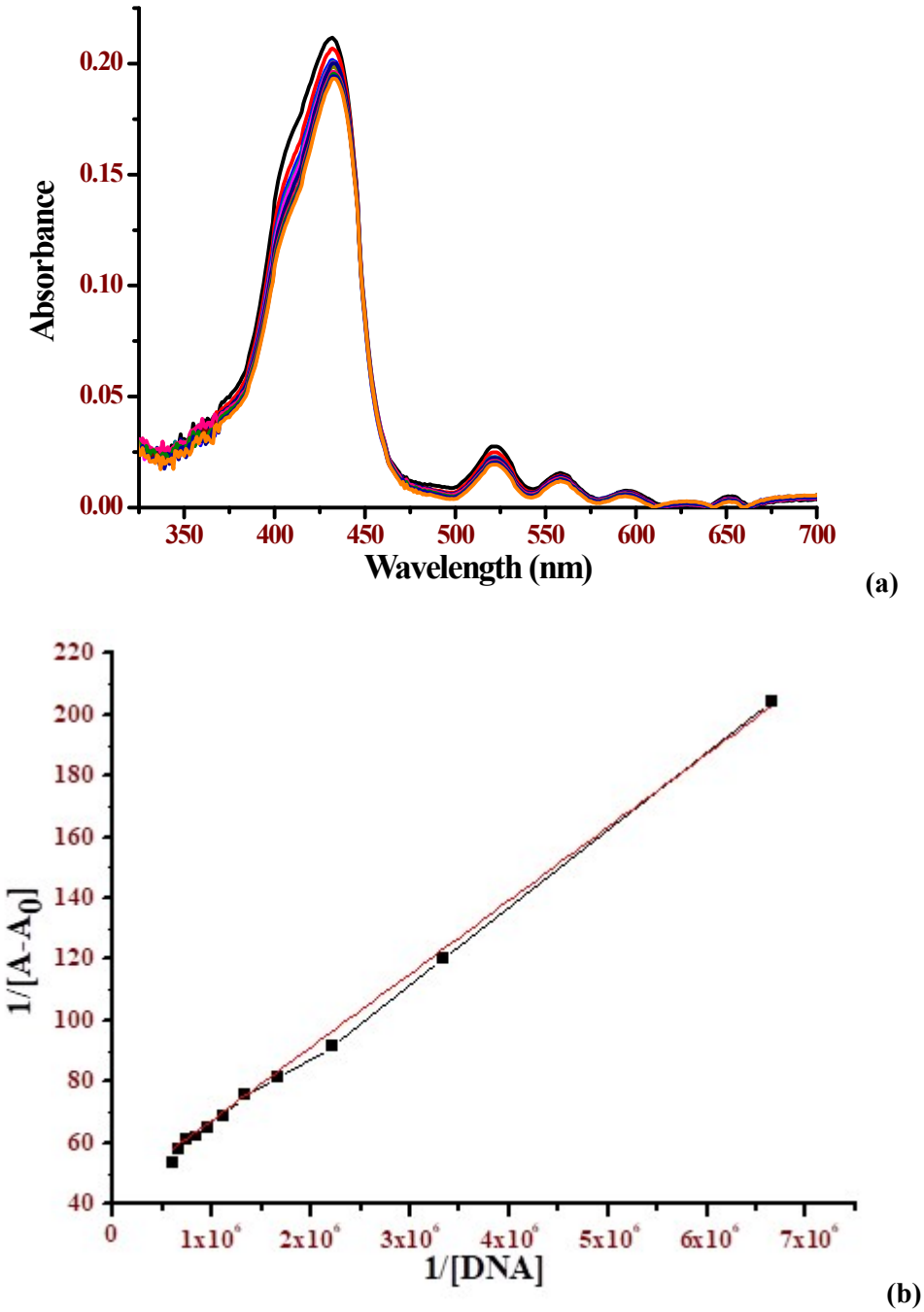

Figure S16. (a) UV-vis titrations of **3c** with ds12; **(b)** corresponding Benesi–Hildebrand plot (linear adjustment in red).

Modelling studies

Modelling of the binding of 3b and 3c to c-Kit2

All optimisations reported in the manuscript were carried out using standard DFT methods as implemented in Gaussian 16.[5] All initial explorations of minima and transition structures were performed at the B3LYP/6-31G*[6,7] level of theory in a SMD solvent model (water) at 298 K in order to mimic experimental conditions.

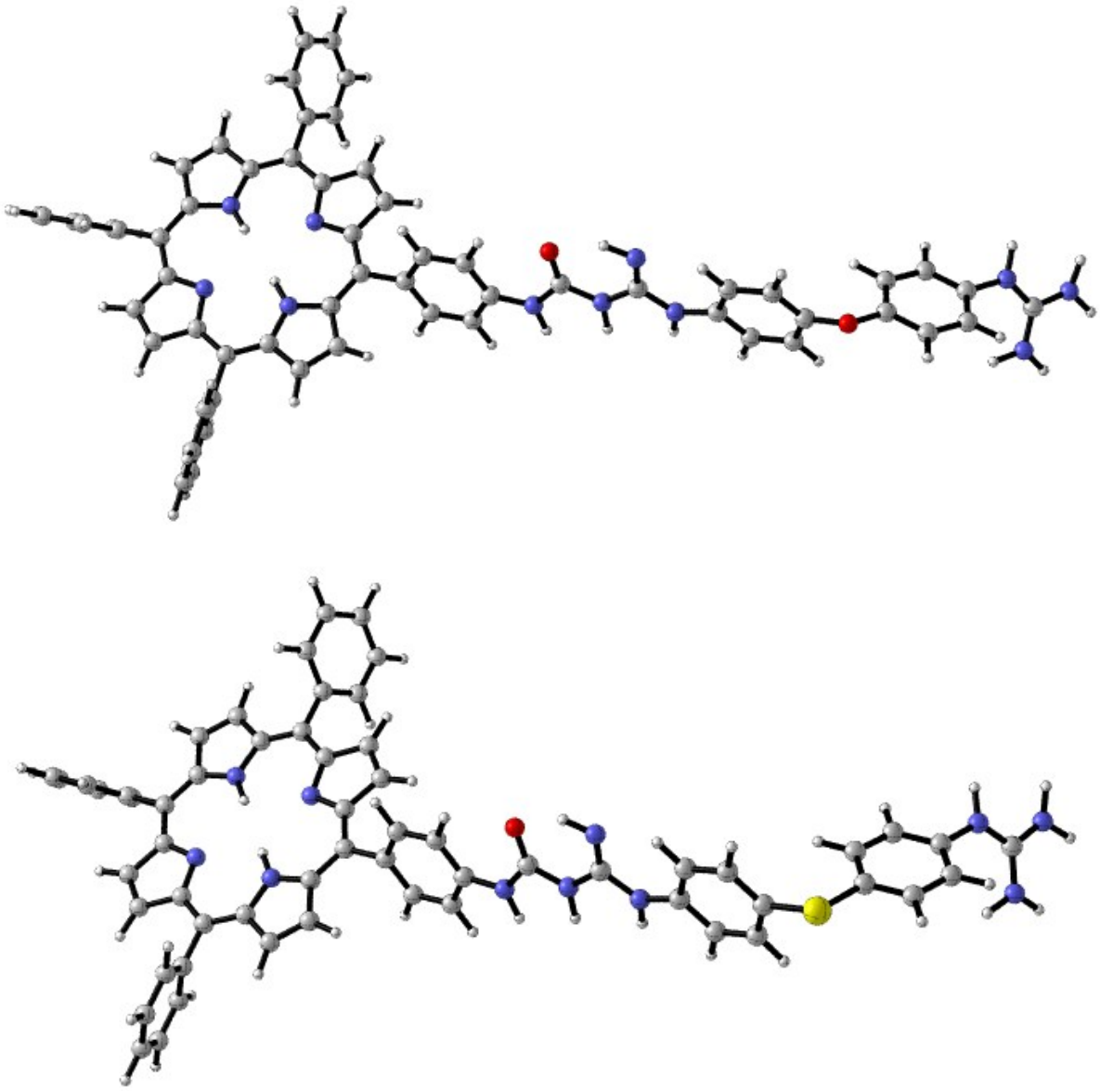

Figure S17. Optimized structures of **3b** (top) and **3c** (bottom) at B3LYP/6-31G*, using SDM-water to model solvation

Docking experiments of the **3b** and **3c** conjugates to the crystal structure of c-Kit2 (2KYP.pdb) were performed by the AutoDock Vina 1.1.2 modelling software.[8]

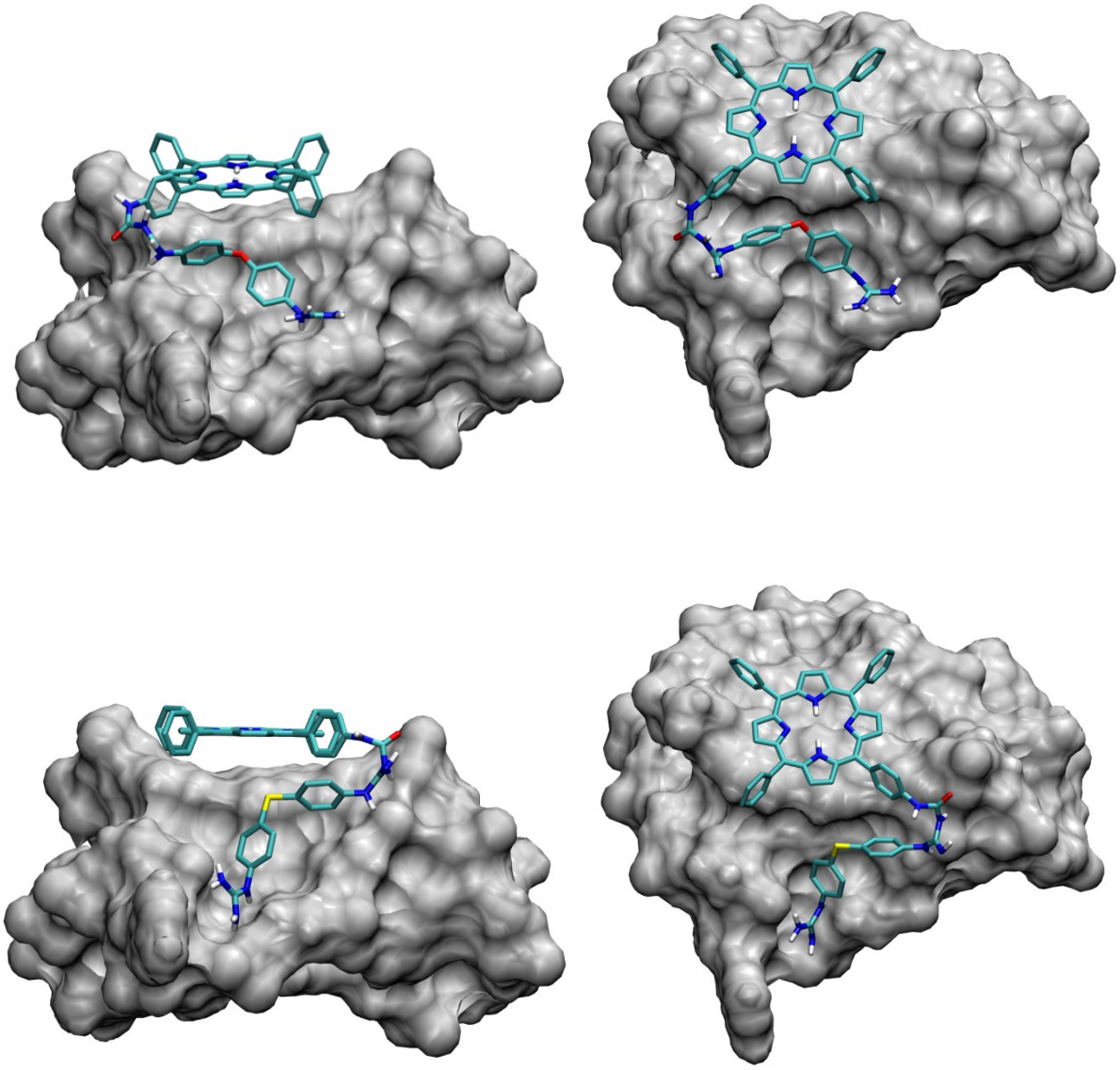

Figure S18. Optimal pose for the docking of **3b** (top) and **3c** (bottom) to c-Kit2

Table S3. Calculated binding affinity G-scores (kcal/mol)

	Affinity
3b	-7.3
3c	-7.4

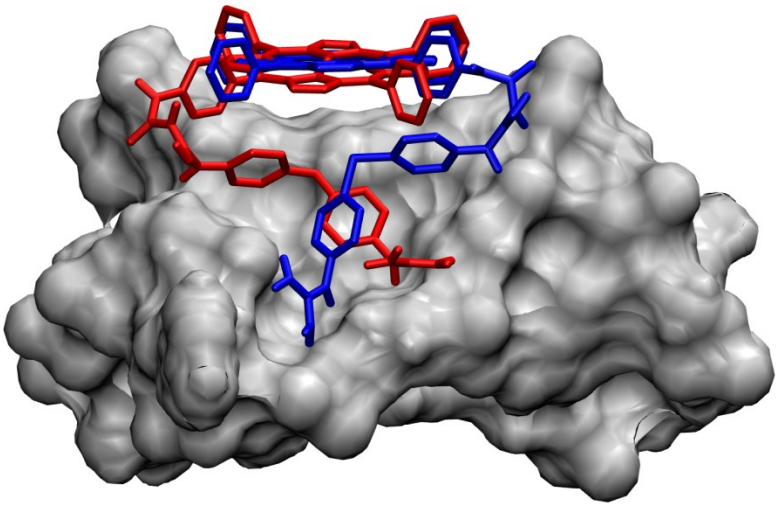

Figure S19. Optimal pose for the docking of **3b** (red) and **3c** (blue) to c-Kit2 superimposed.

Modelling of the binding of 3a and 3e, and their metallated derivatives 4a and 4e to c-Kit2

Different effects are observed in the binding of conjugates **3a** and **3e** and their corresponding Zn complexes **4a** and **4e** to c-Kit2 in the UV-thermal melting experiments. Thus, while **4a** seems to binds stronger to c-Kit2 than **3a**, the opposite occurs for **3e** and **4e**. First, structural differences between **3,4a** and **3,4e** could explain the different binding; thus, compounds **3a** and **4a** have a CH_2 linker in the diaromatic guanidine moiety, whereas **3e** and **4e** have a more flexible CH_2CH_2 linker that will probably result in a different mode of binding and then the effect of metallation in these two series may have different effects on the affinity. Thus, in order to understand these effects, docking studies have been performed with these four conjugates and the c-Kit2 model. Considering all the limitations that the docking methodology involve, we observed that in the case of compounds **3e** and **4e** the chains of the ethylene linker in fact interact with different parts of the loops than the methylene-linked derivatives **3a** and **4a** (see Figures S20 and S21).

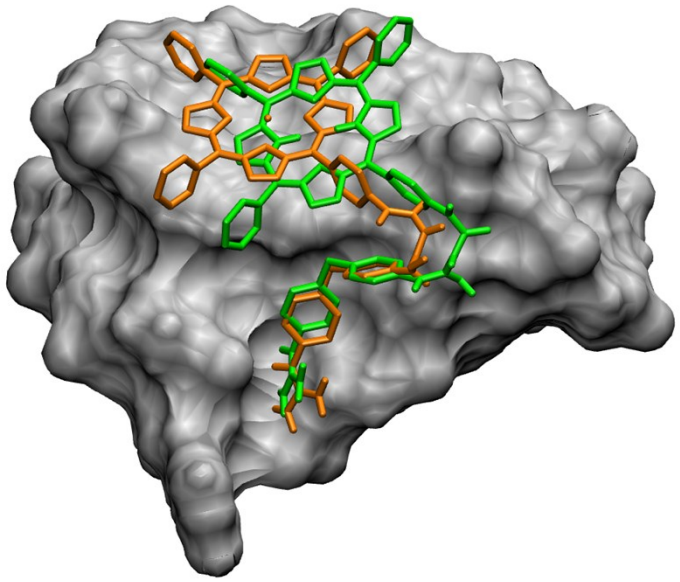

Figure S20. Optimal pose for the docking of **3a** (green) and **4a** (orange) to c-Kit2 superimposed.

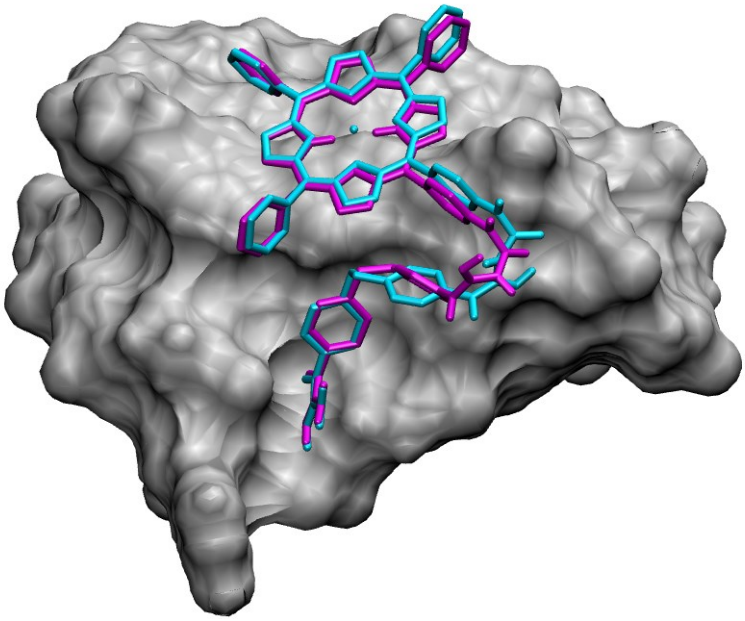

Figure S21. Optimal pose for the docking of **3e** (magenta) and **4e** (blue) to c-Kit2 superimposed.

Looking at the binding energy G-scores obtained in these docking studies, we observe the following order: **4a** (-8 kcal/mol) > **3a** (-7.8 kcal/mol) > **3e** (-7.5 kcal/mol) > **4e** (-7.4 kcal/mol). Therefore, in agreement to the experimental results, these docking studies indicate that the metallation of **3a** has a deeper effect in the binding than that of **3e**. This is observed not only in the G-scores (which we acknowledge have not real thermodynamical meaning), but also in the orientation of the porphyrin moiety over the upper tetrad since the metallated porphyrin core of **4a** (orange in Figure S22) is more centred over the G-tetrad than that the rest of the conjugates studied (**4e** blue, **3a** green, **3e** magenta, in Figure S22).

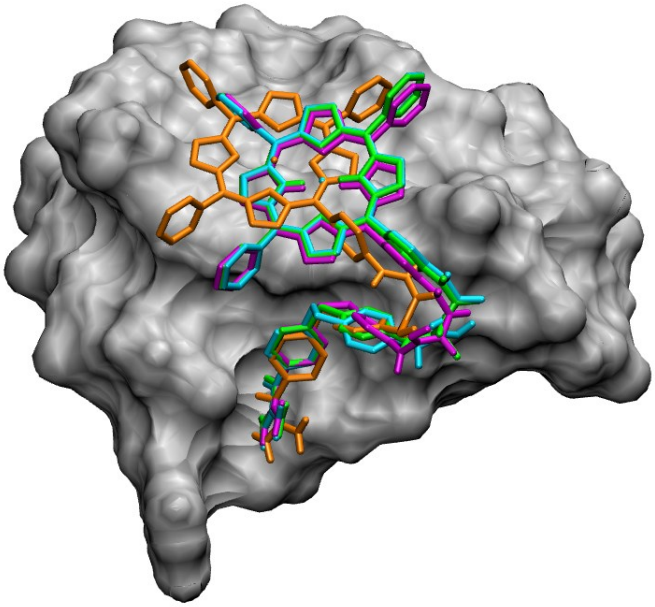

Figure S22. Optimal pose for the docking of **3a** (green), **3e** (magenta), **4a** (orange) and **4e** (blue) to c-Kit2 superimposed.

Purity assessment of final compounds

The HPLC purity analysis of prepared ligands was carried out using Alliance 2695 HPLC system (Waters Corporation, Milford, MA, USA) equipped with PDA detector and automatic injector (5 µL). The stationary phase consist of Atlantis T3 C18 column (Waters Corporation, Milford, USA, 100 mm × 2.1 mm; 3 µm particle size) and elution was carried out using stepwise gradient system, eluting at 0.3 mL/min: acetonitrile (A) and aqueous formate buffer (30 mM, pH 3.0, B) starting with A:B (50:50) to (100: 0) for 30 min. The compounds analysed were found to be >95% pure.

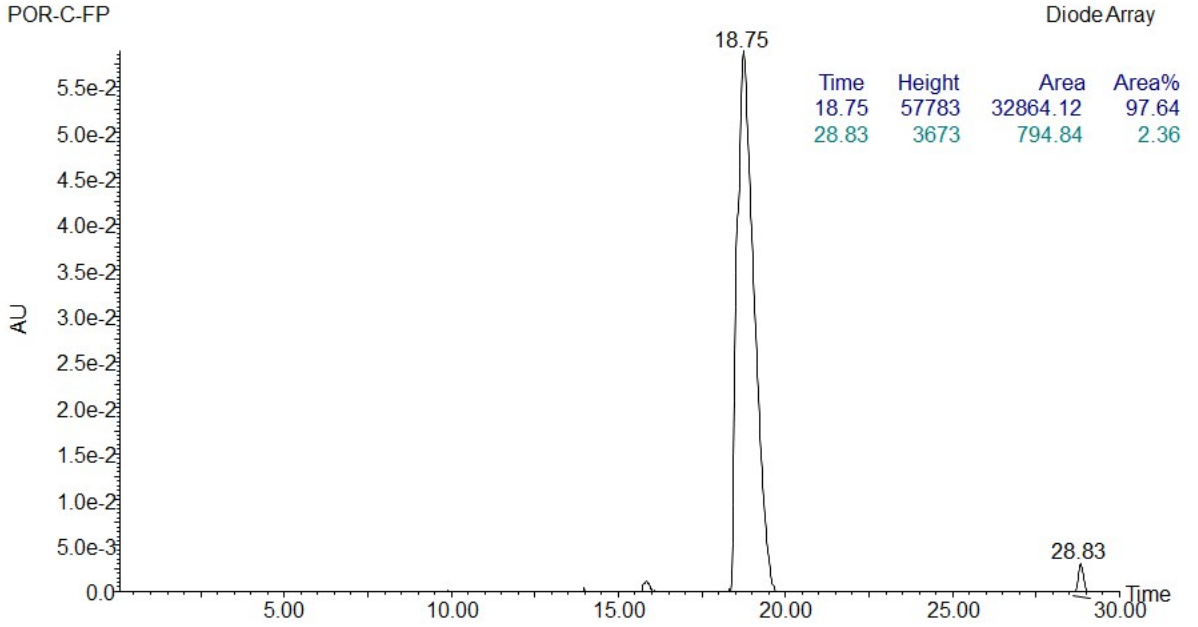

Figure S20. HPLC profile of **3a**.

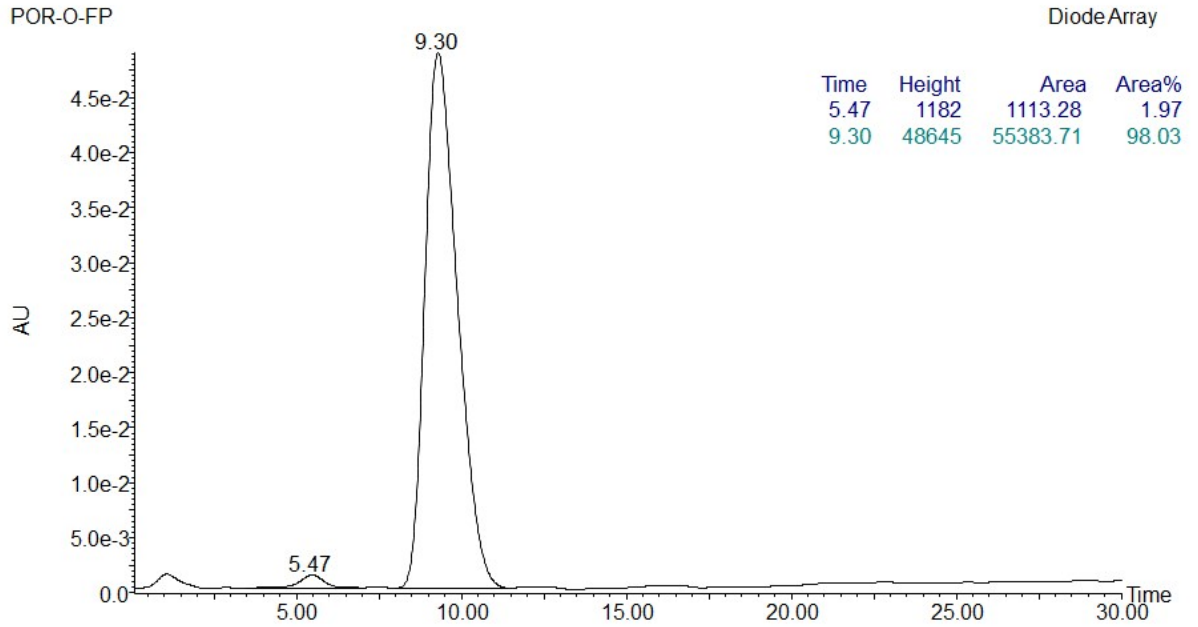

Figure S21. HPLC profile of **3b**.

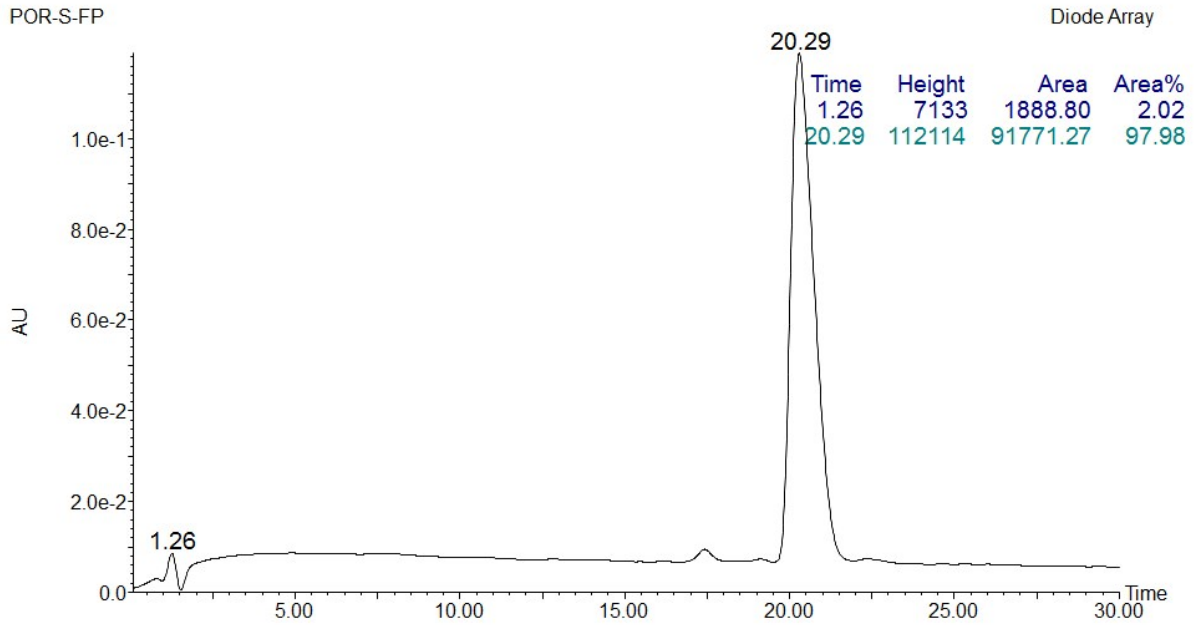

Figure S22. HPLC profile of **3c**.

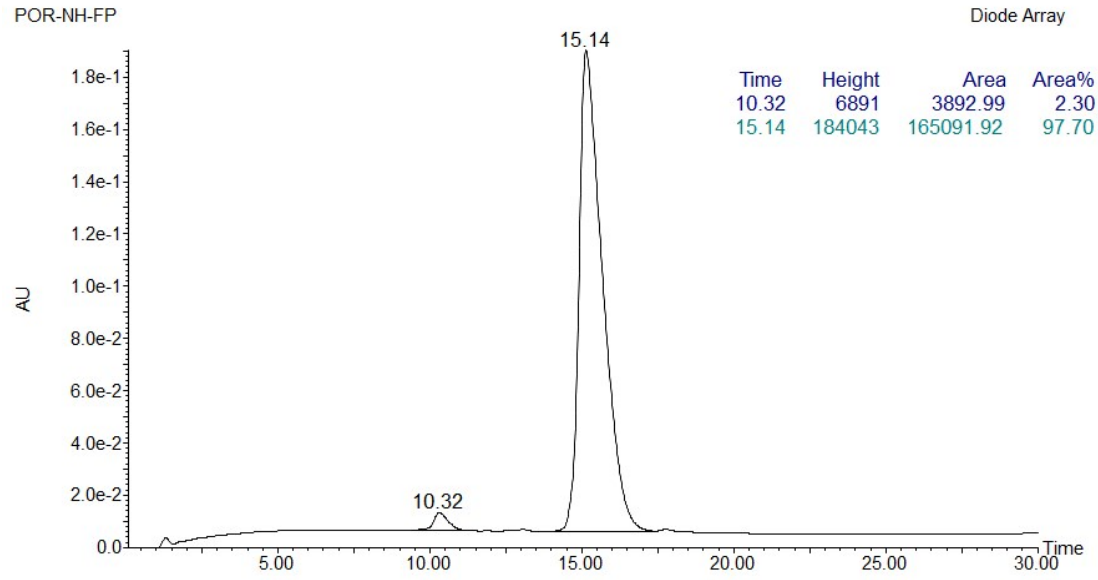

Figure S23. HPLC profile of **3d**.

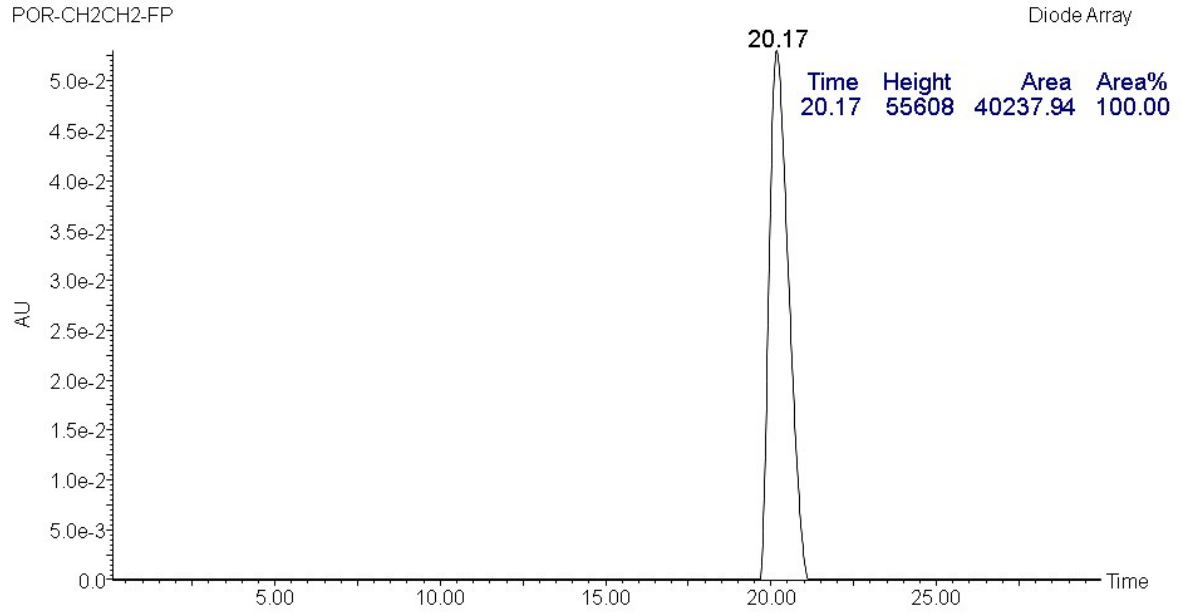

Figure S24. HPLC profile of **3e**.

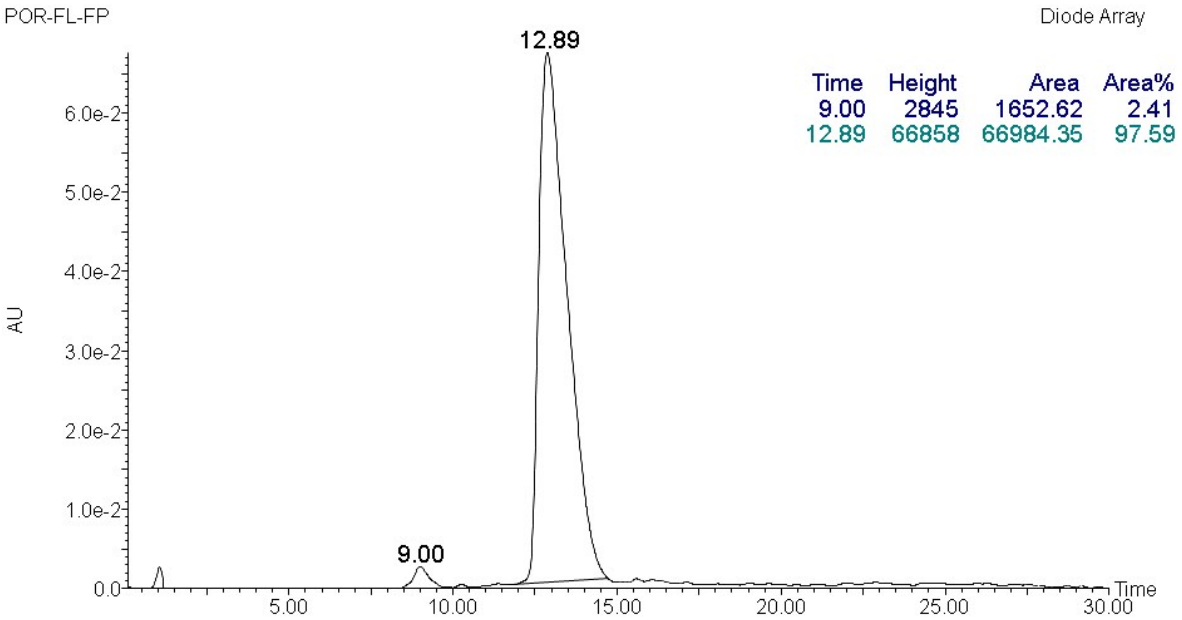

Figure S25. HPLC profile of **3f**.

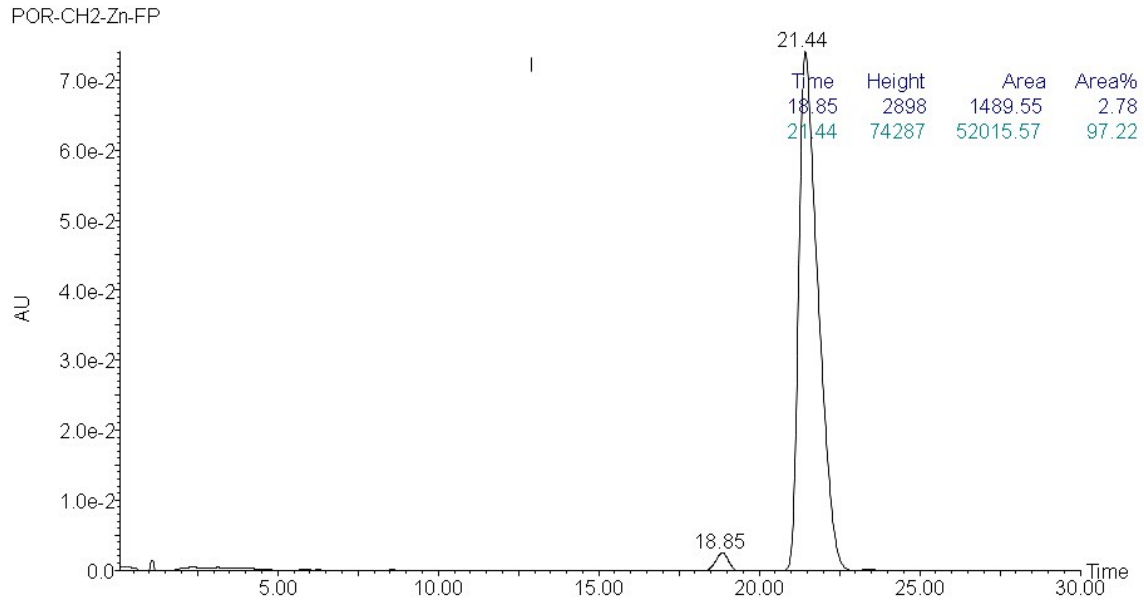

Figure S26. HPLC profile of **4a**.

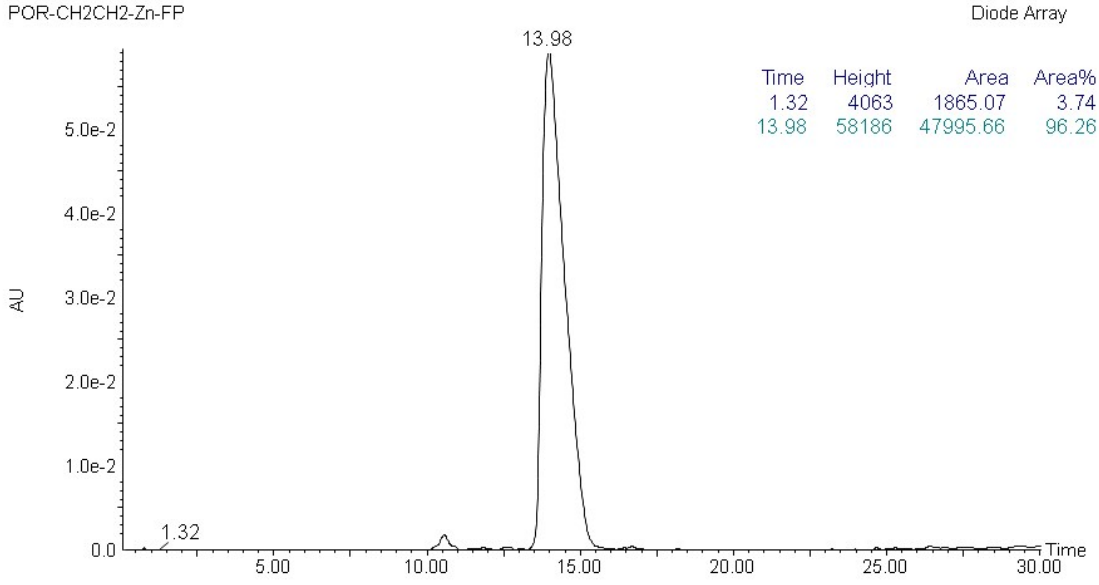

Figure S27. HPLC profile of **4e**.

^{1}H and ^{13}C NMR Spectra of new compounds

2a: ^{1}H NMR ($CDCl_3$) ^{13}C NMR ($CDCl_3$)

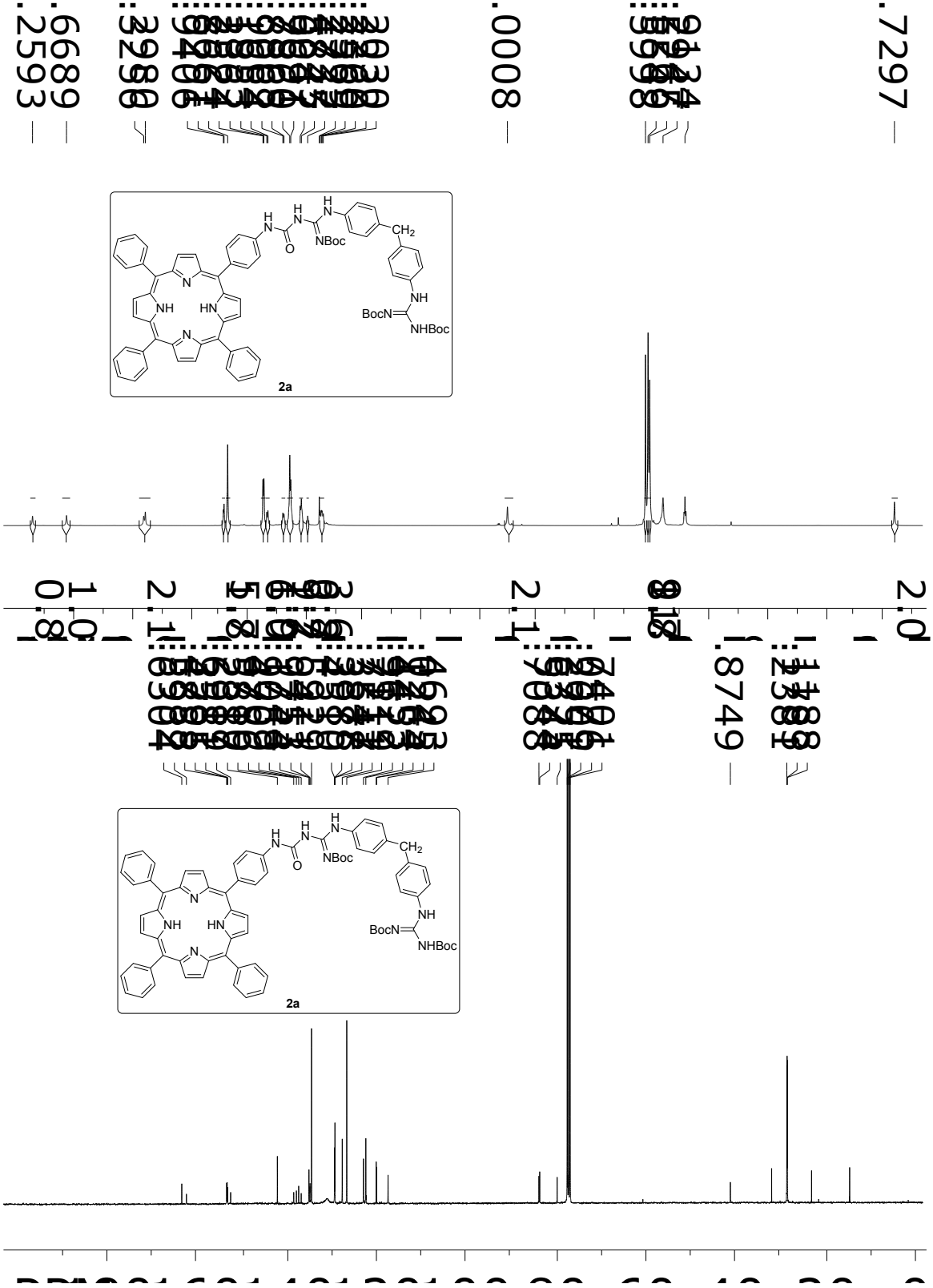

2b: ^{1}H NMR ($CDCl_3$) ^{13}C NMR ($CDCl_3$)

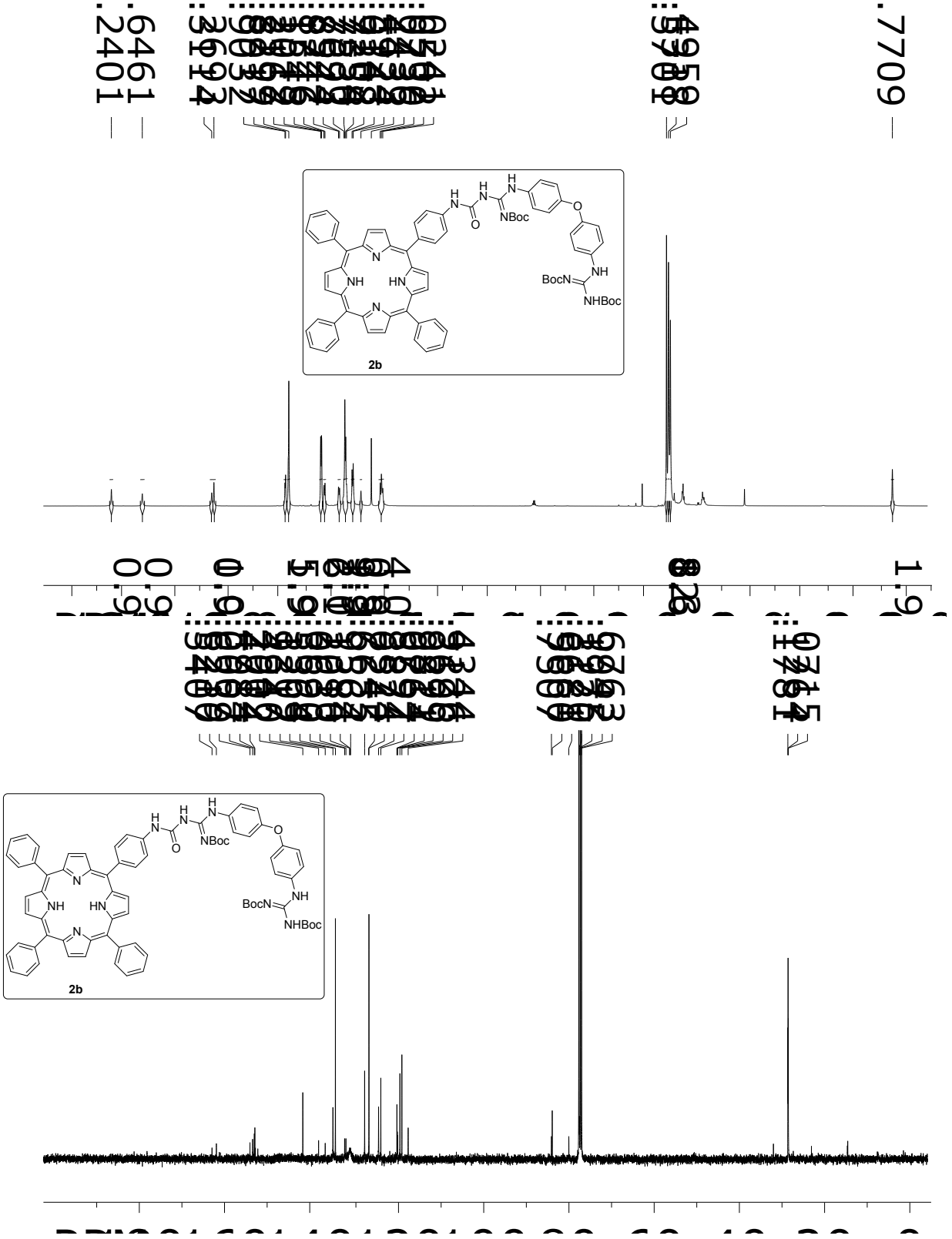

2c: ^{1}H NMR ($CDCl_3$) ^{13}C NMR ($CDCl_3$)

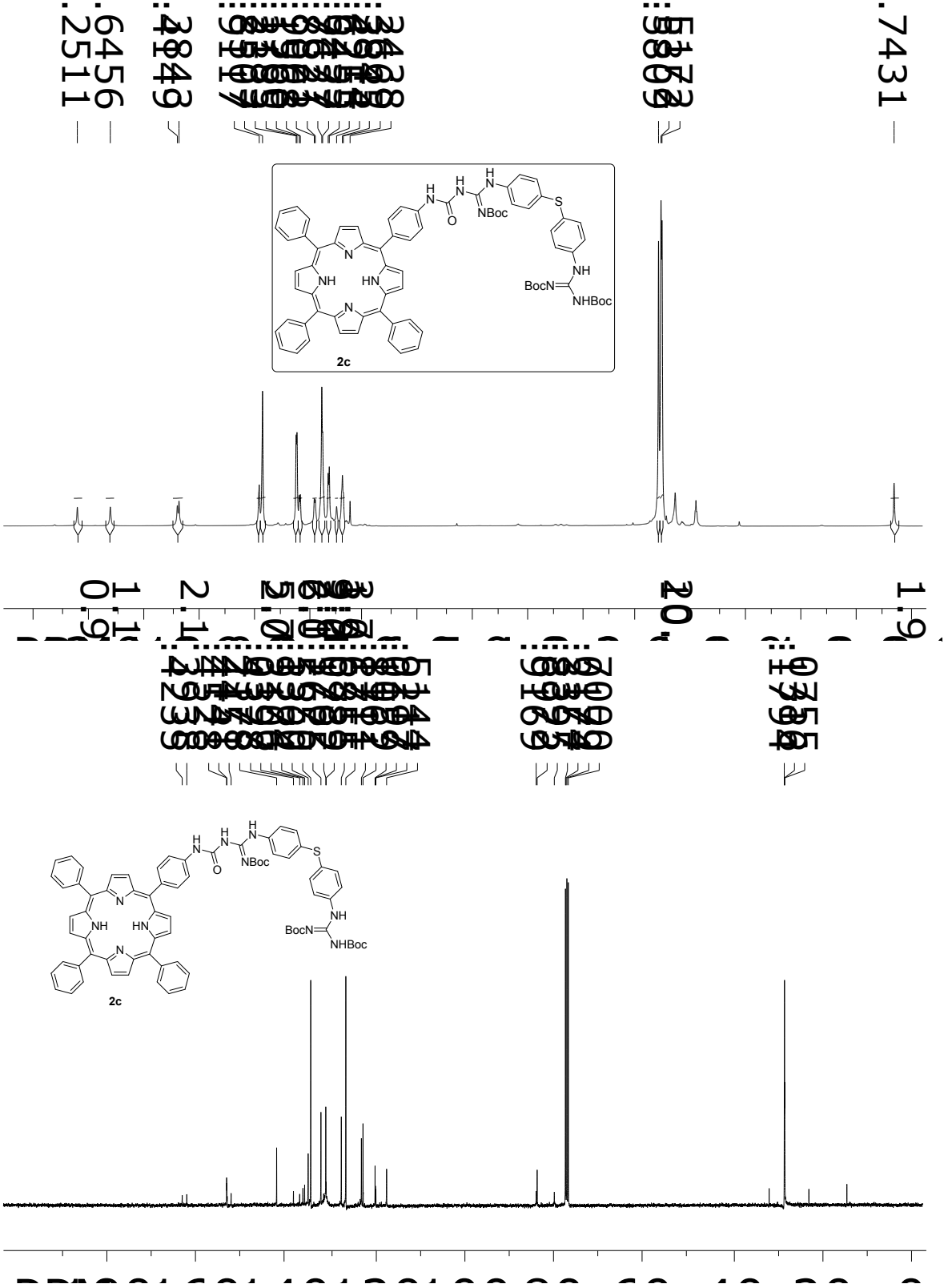

2e: ^{1}H NMR ($CDCl_3$) ^{13}C NMR ($CDCl_3$)

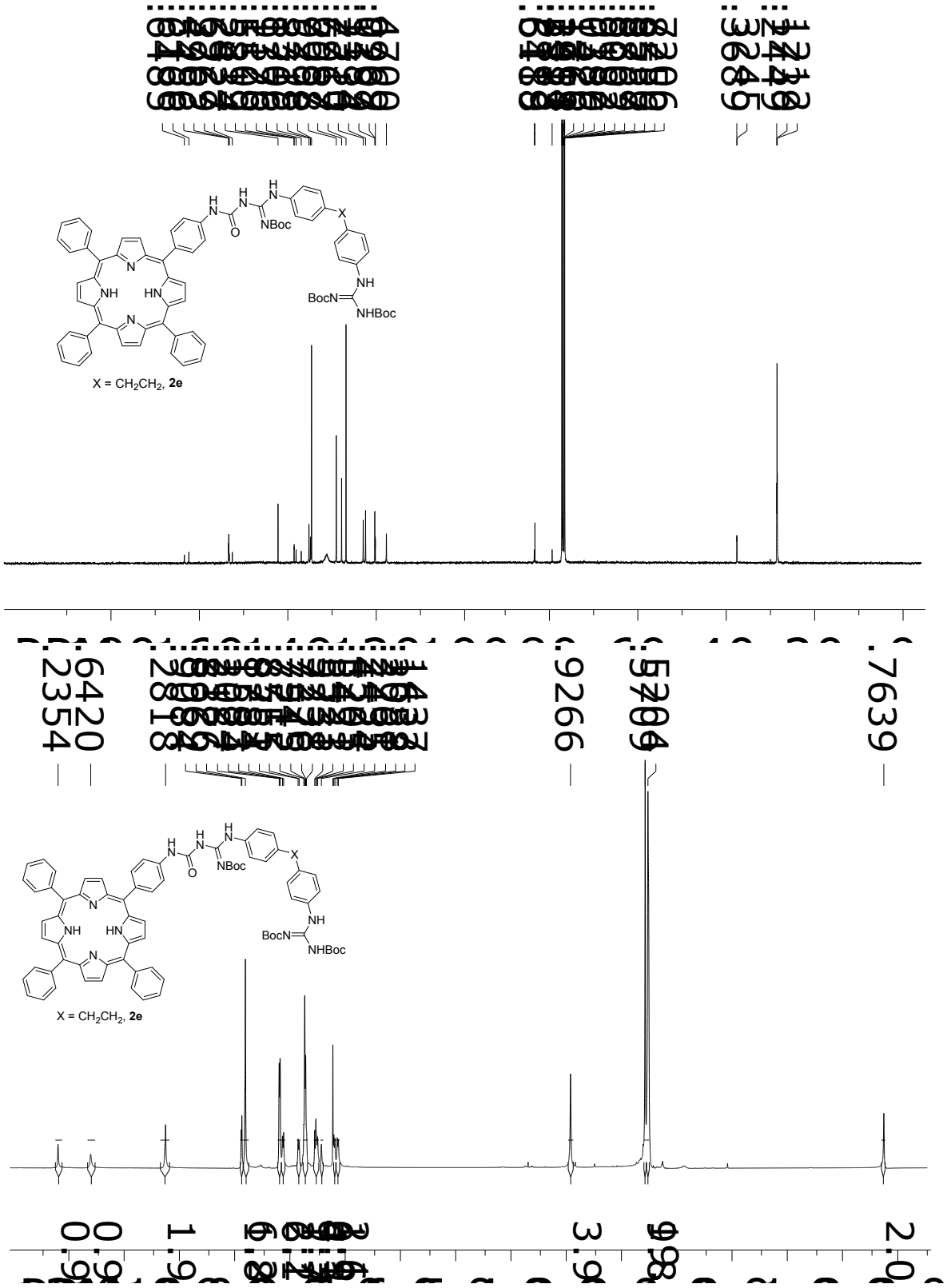

2f: ^{1}H NMR ($CDCl_3$) ^{13}C NMR ($CDCl_3$)

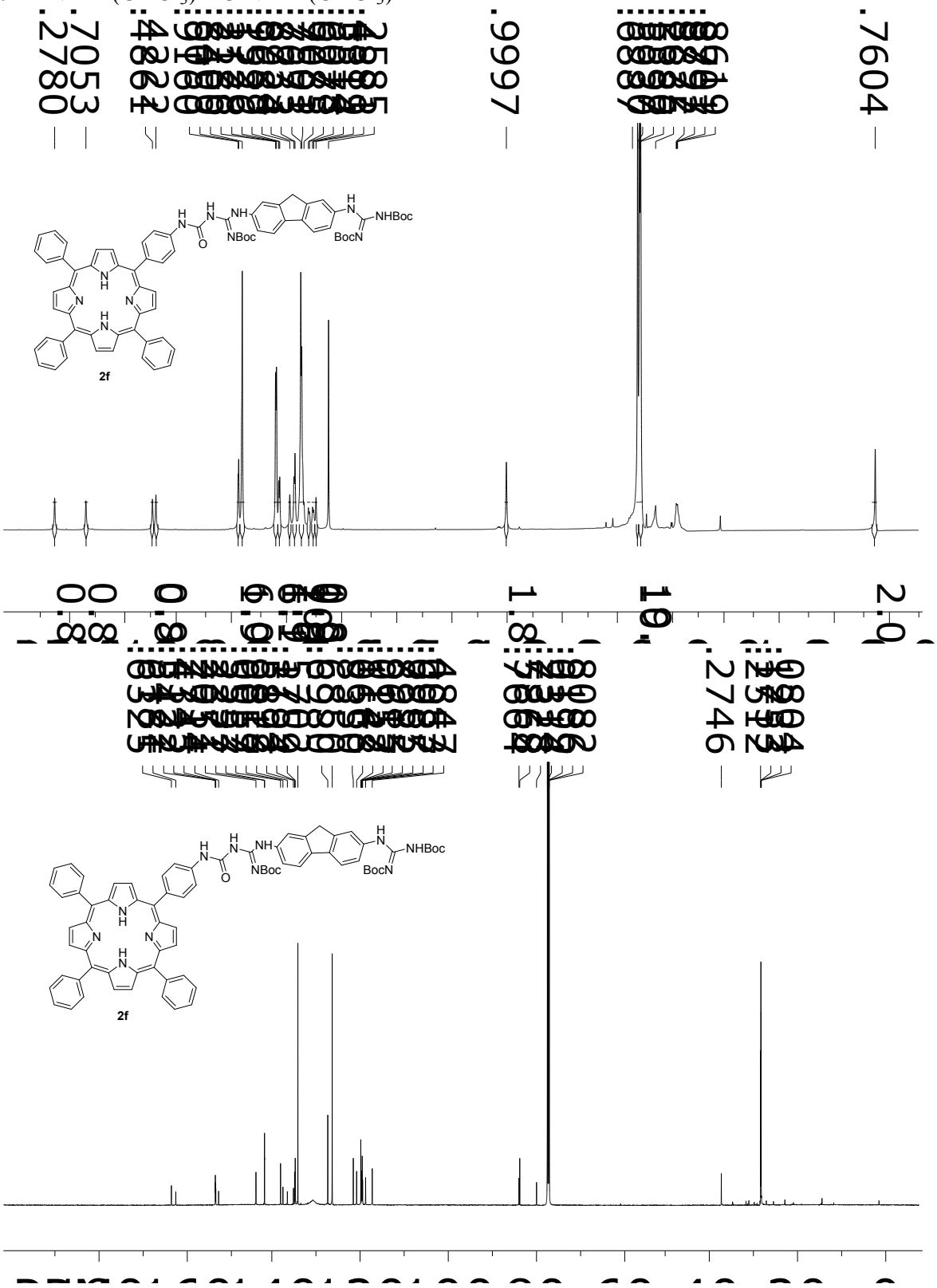

3a: ^{1}H NMR (MeOD) ^{13}C NMR (MeOD)

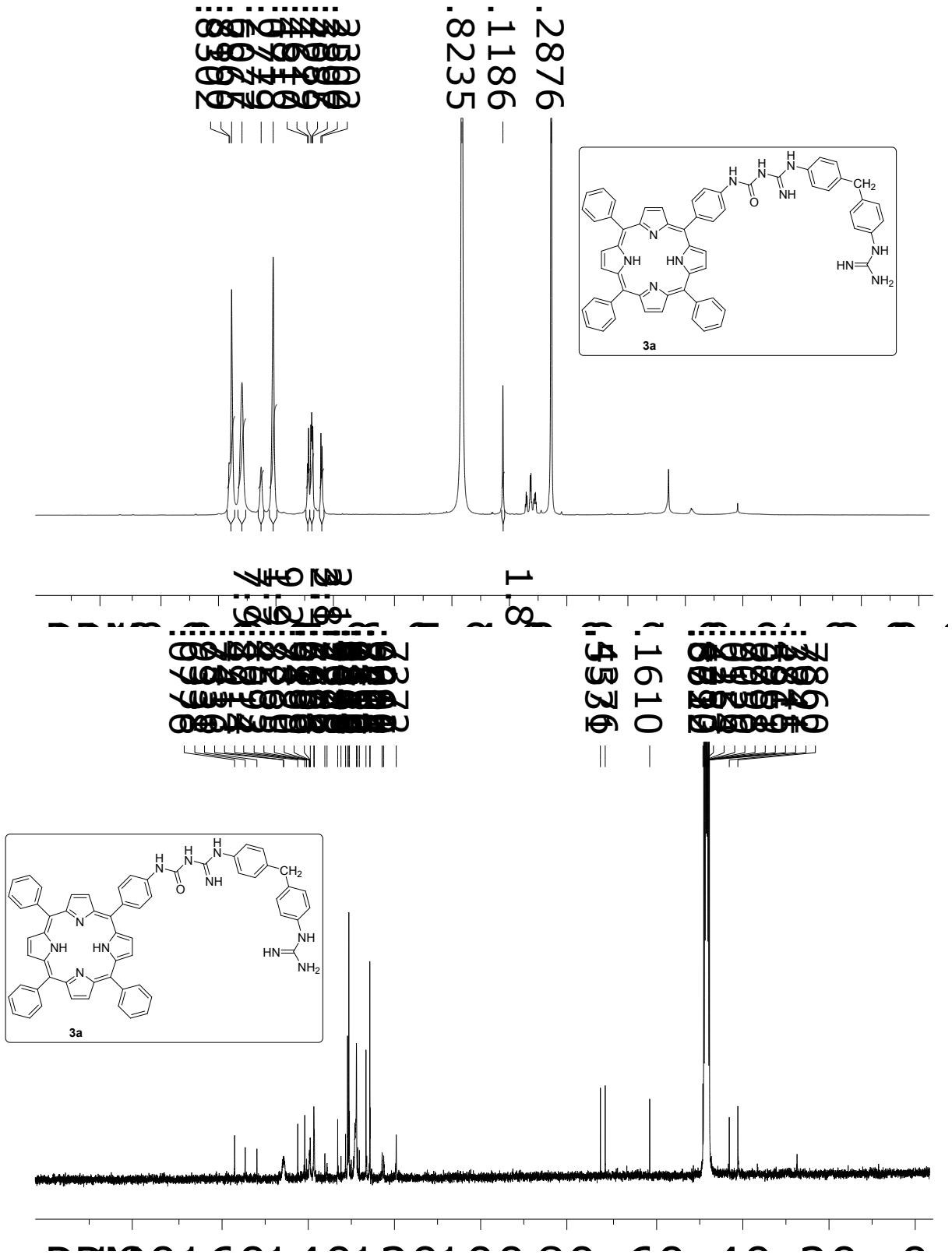

3b: ^{1}H NMR (MeOD) ^{13}C NMR (MeOD)

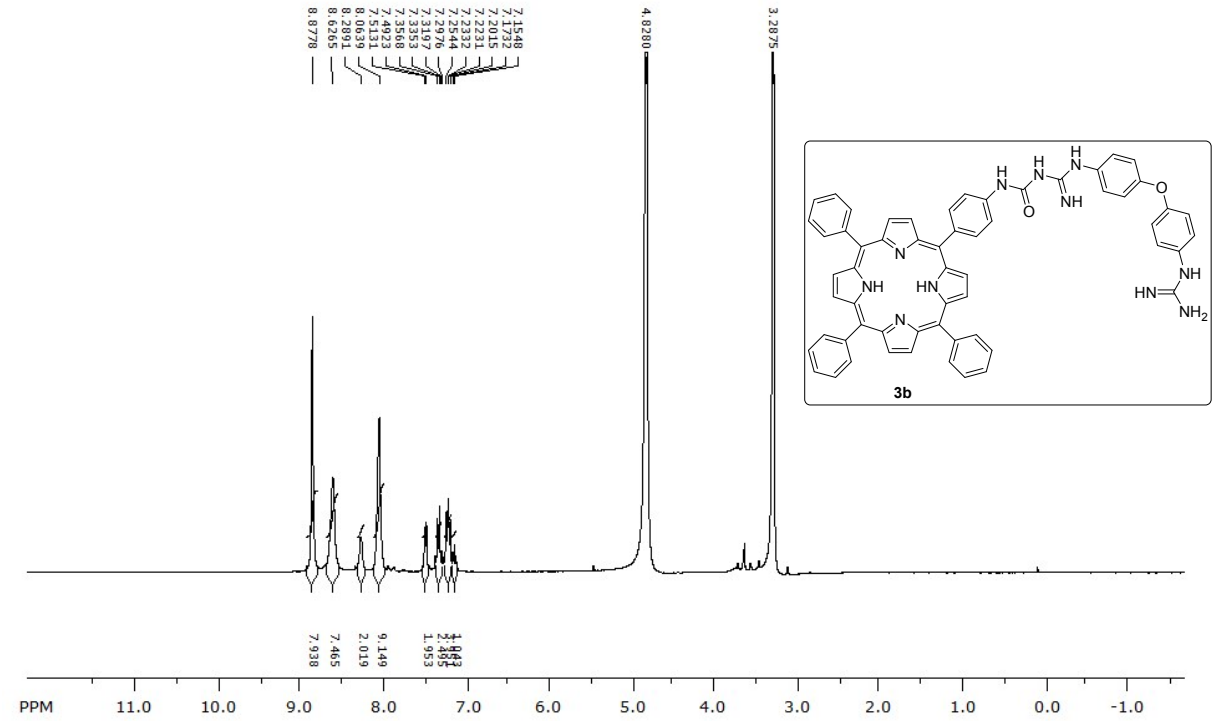

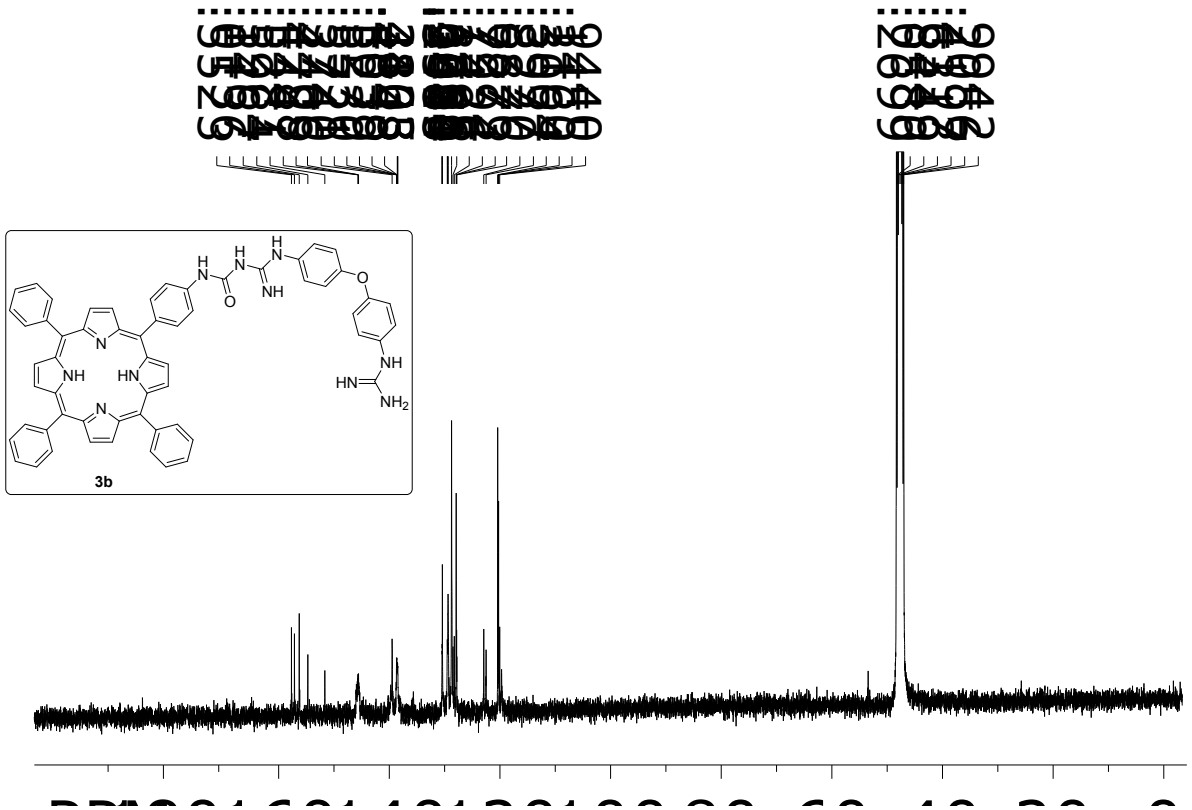

3c: ^{1}H NMR (MeOD) ^{13}C NMR (MeOD)

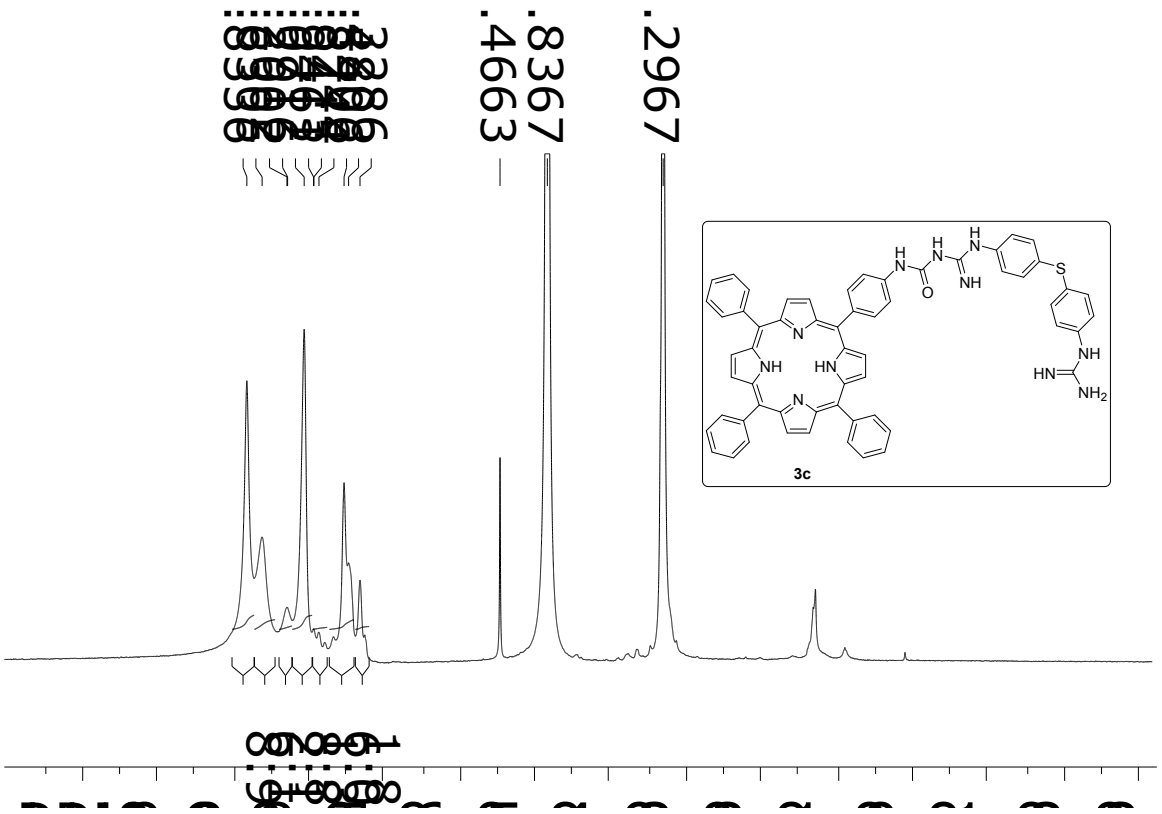

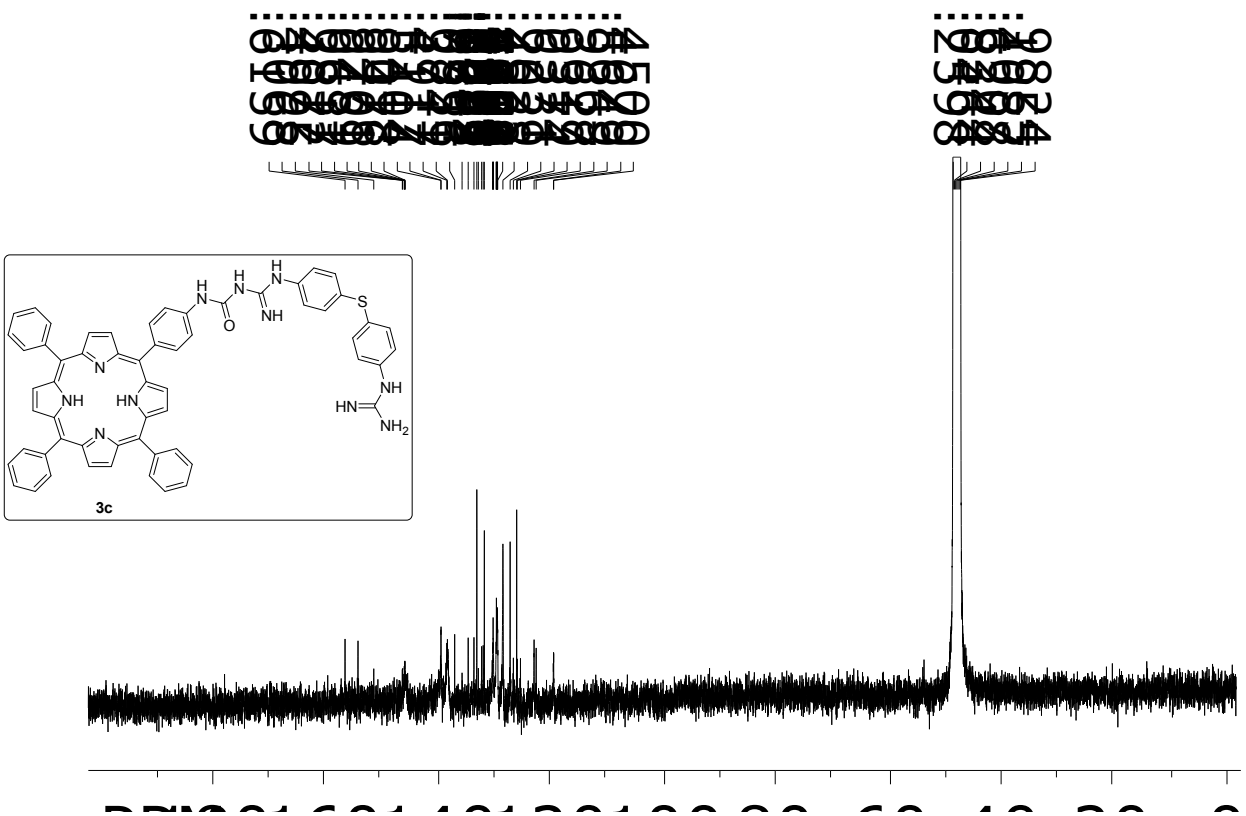

3d: ^{1}H NMR (MeOD) ^{13}C NMR (MeOD)

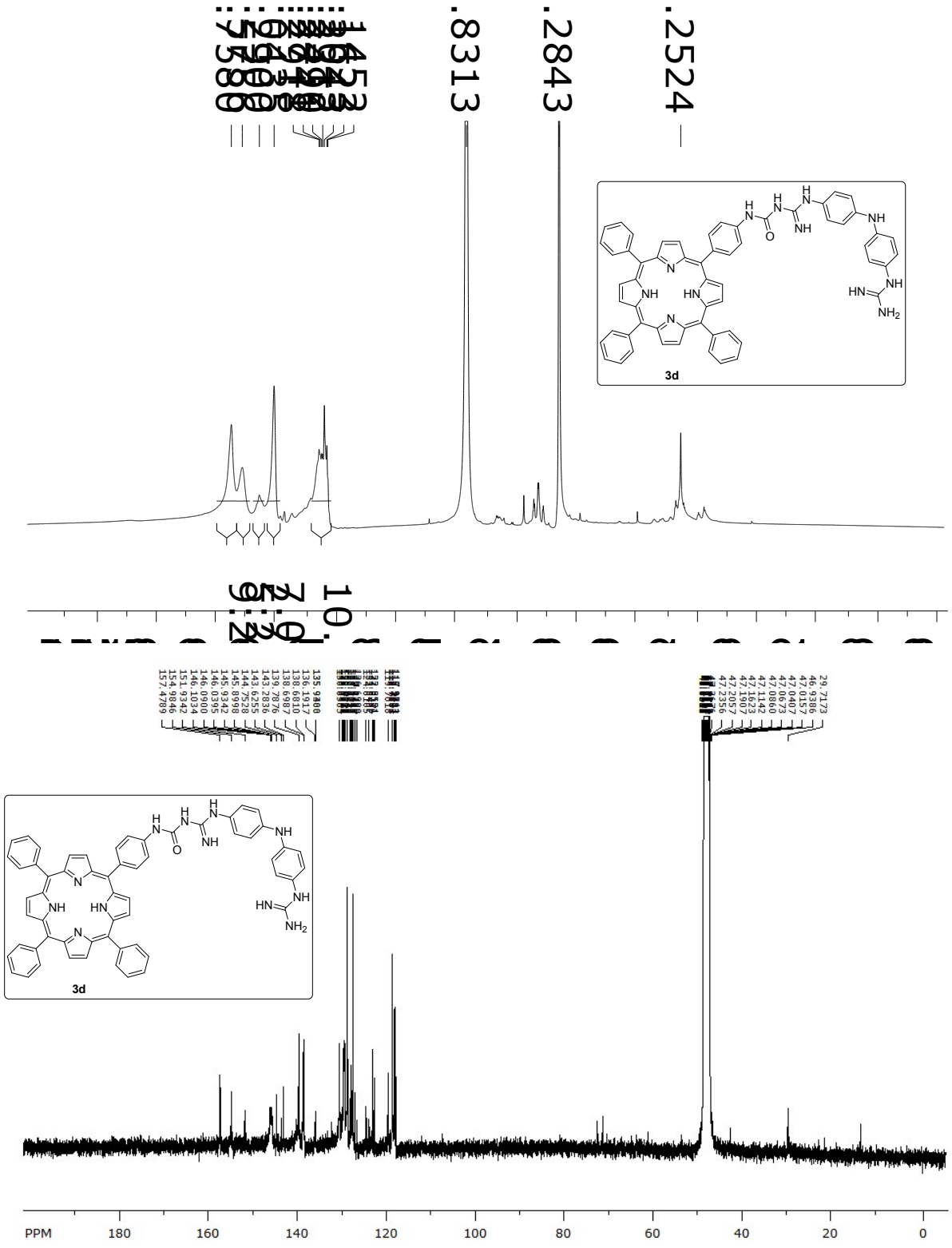

3e: ^{1}H NMR (MeOD) ^{13}C NMR (MeOD)

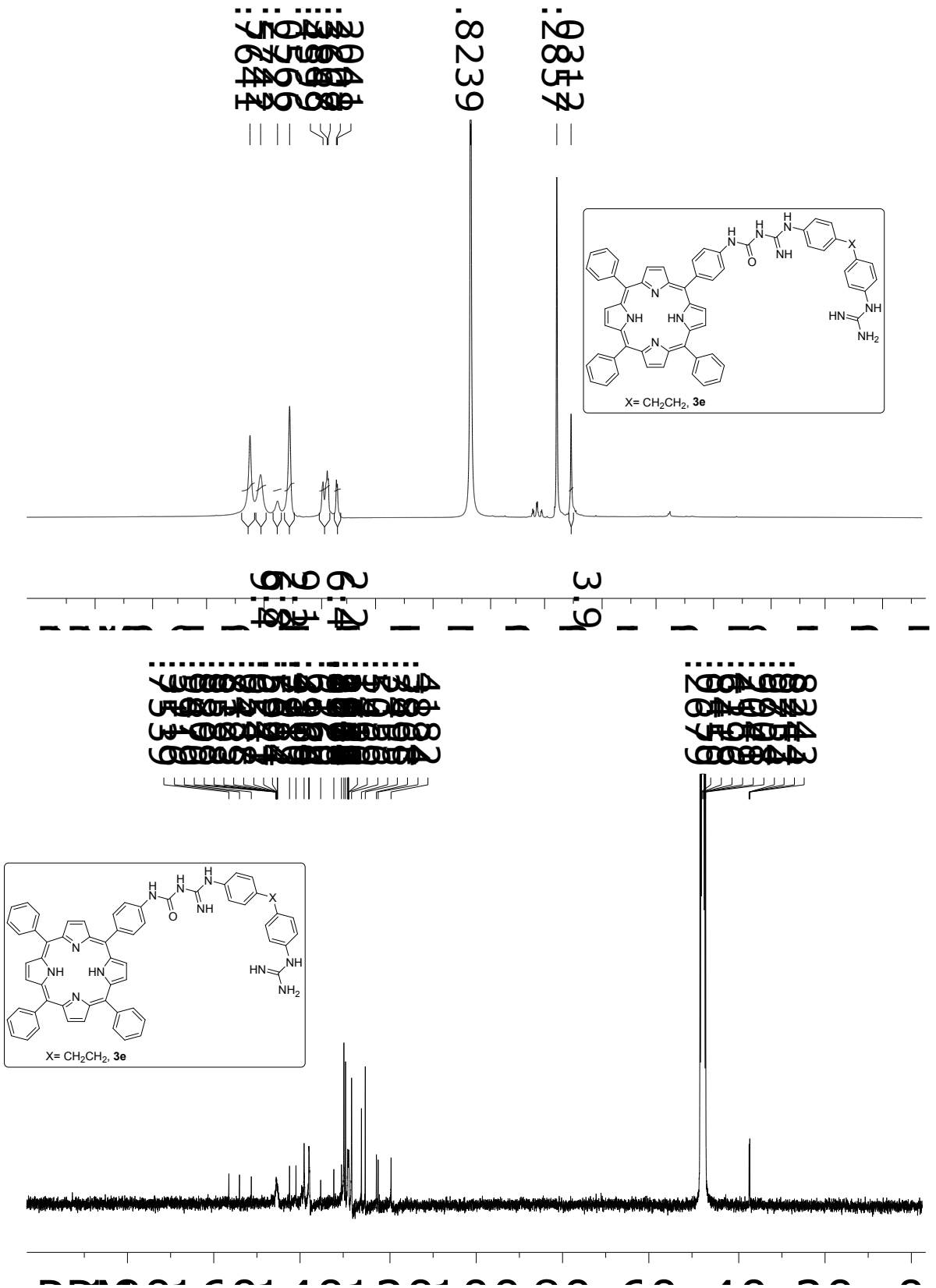

3f: ^{1}H NMR (MeOD) ^{13}C NMR (MeOD)

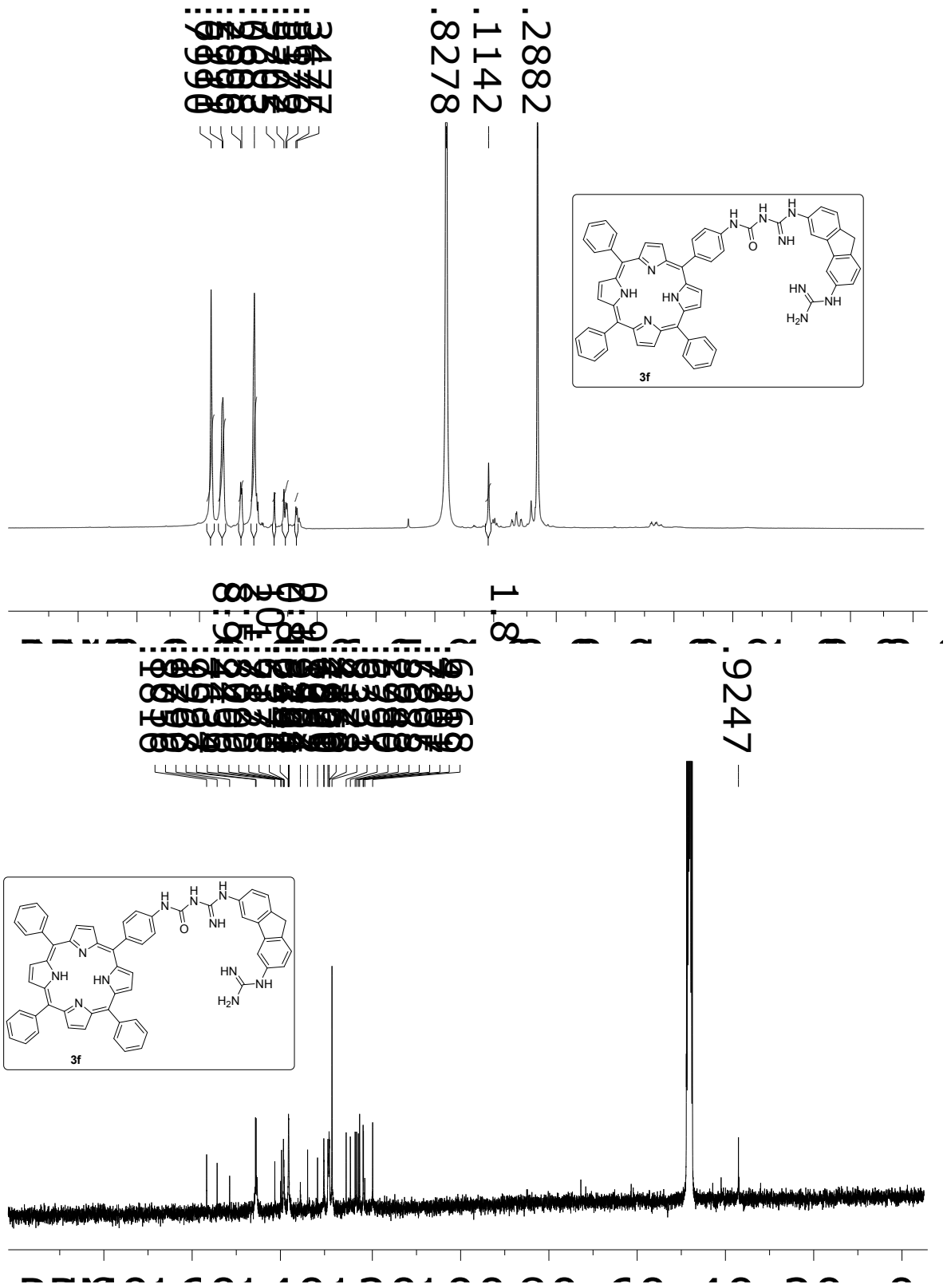

4a: ^{1}H NMR (MeOD) ^{13}C NMR (MeOD)

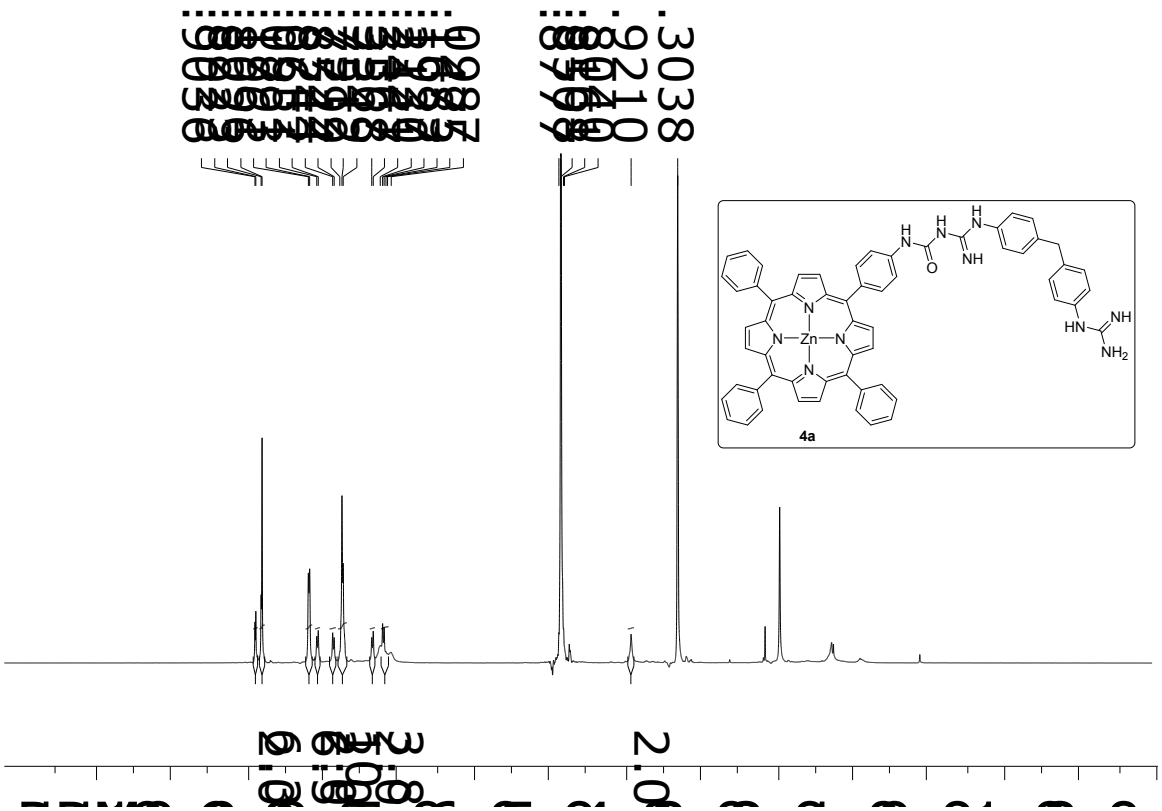

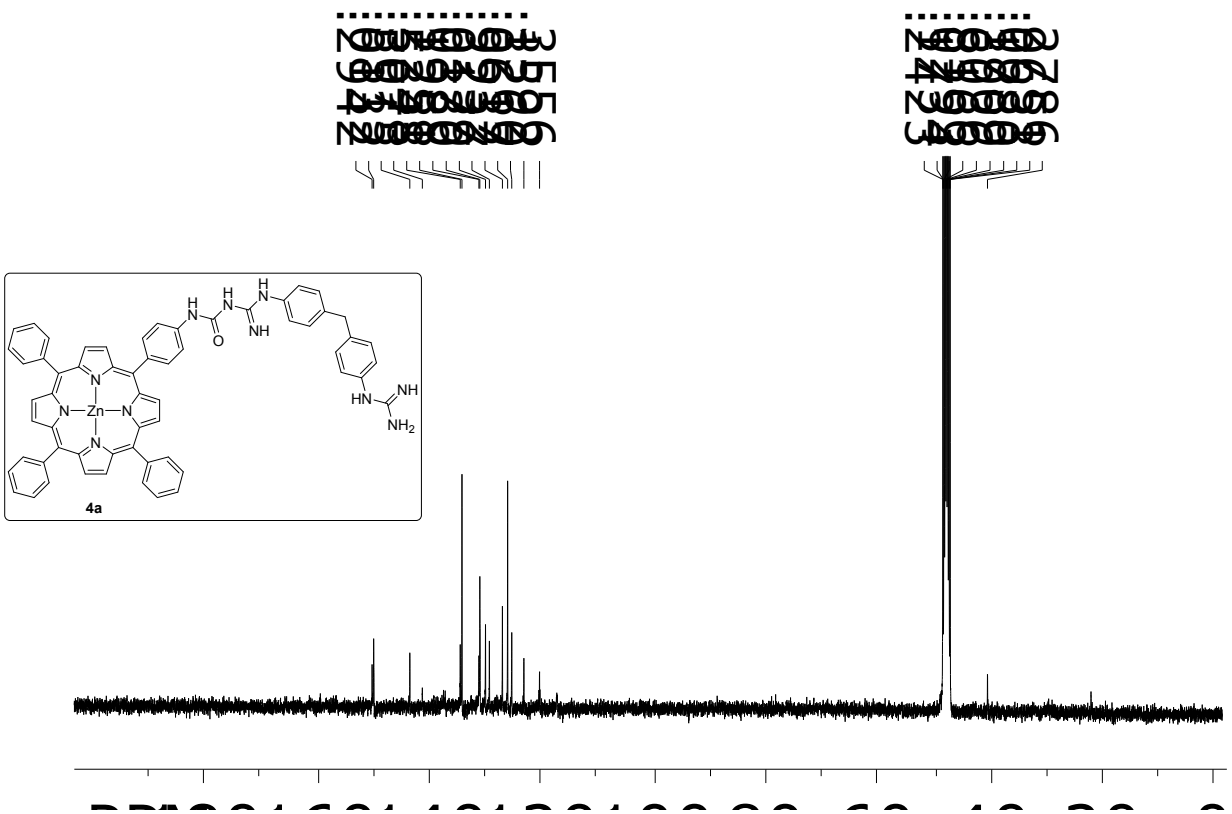

4e: ^{1}H NMR (MeOD) ^{13}C NMR (MeOD)

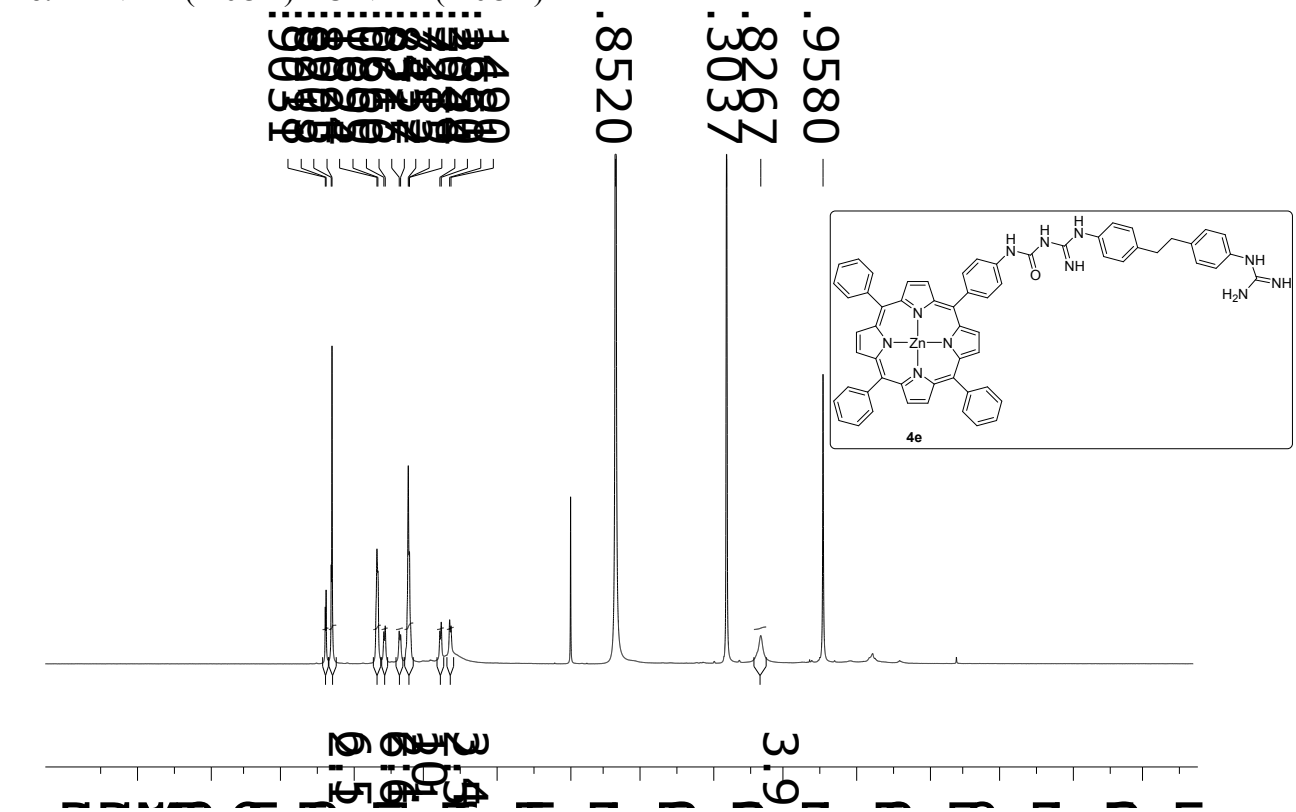

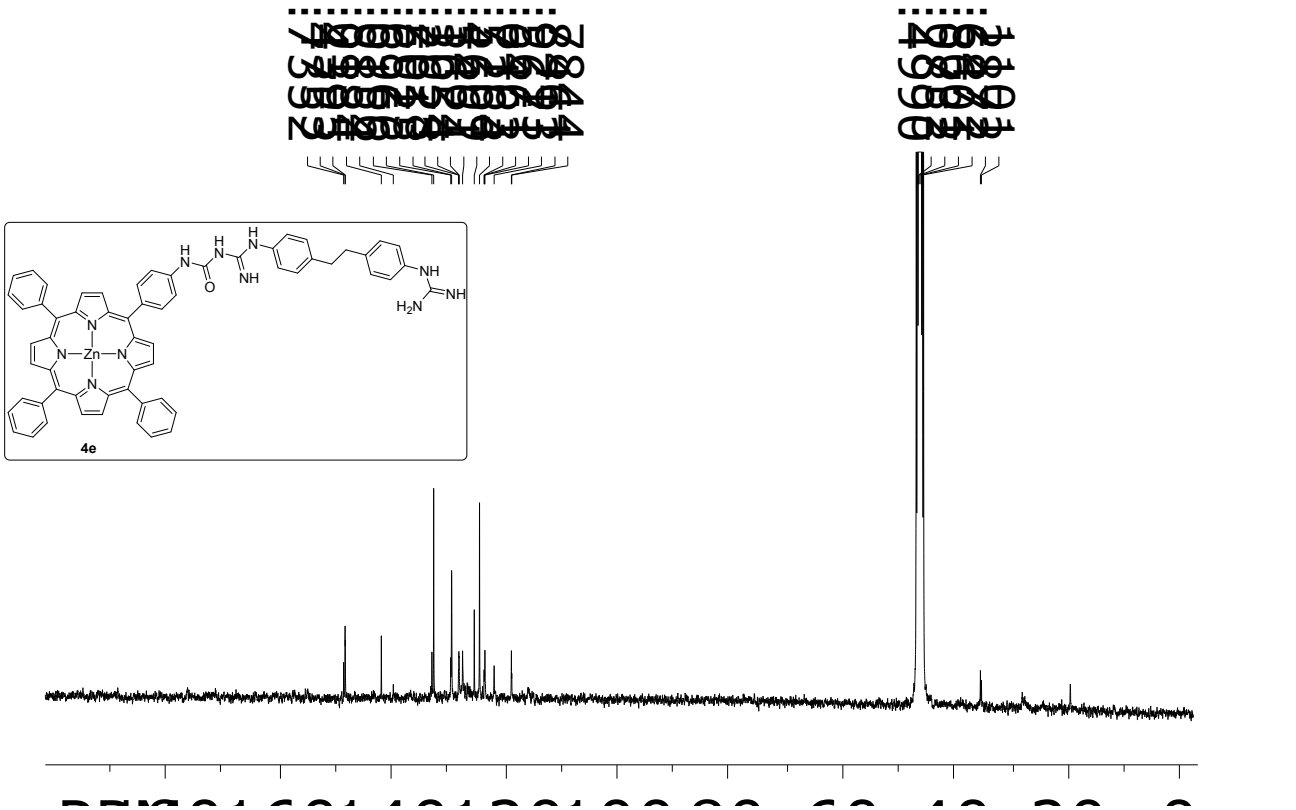

References

1. H. E. Gottlieb, V. Kotlyar, A. Nudelman, *J. Org. Chem.* 1997, **62**, 7512.
2. R. Luguya, L. Jaquinod, F. R. Fronczek, M. G. H. Vicente, K. M. Smith, *Tetrahedron* 2004, **60**, 2757.
3. For example: a) F. Rodriguez, I. Rozas, M. Kaiser, R. Brun, B. Nguyen, R. N. Garcia, C. Dardonville, *J. Med. Chem.* 2008, **51**, 909; b) C. McKeever, M. Kaiser, I. Rozas, *J. Med. Chem.* 2013, **56**, 700.
4. Origin (OriginLab, Northampton, MA)
5. Gaussian 16, M. J. Frisch, G. W. Trucks, H. B. Schlegel, G. E. Scuseria, M. A. Robb, J. R. Cheeseman, G. Scalmani, V. Barone, G. A. Petersson, H. Nakatsuji, X. Li, M. Caricato, A. V. Marenich, J. Bloino, B. G. Janesko, R. Gomperts, B. Mennucci, H. P. Hratchian, J. V. Ortiz, A. F. Izmaylov, J. L. Sonnenberg, Williams, F. Ding, F. Lipparini, F. Egidi, J. Goings, B. Peng, A. Petrone, T. Henderson, D. Ranasinghe, V. G. Zakrzewski, J. Gao, N. Rega, G. Zheng, W. Liang, M. Hada, M. Ehara, K. Toyota, R. Fukuda, J. Hasegawa, M. Ishida, T. Nakajima, Y. Honda, O. Kitao, H. Nakai, T. Vreven, K. Throssell, J. A. Montgomery Jr., J. E. Peralta, F. Ogliaro, M. J. Bearpark, J. J. Heyd, E. N. Brothers, K. N. Kudin, V. N. Staroverov, T. A. Keith, R. Kobayashi, J. Normand, K. Raghavachari, A. P. Rendell, J. C. Burant, S. S. Iyengar, J. Tomasi, M. Cossi, J. M. Millam, M. Klene, C. Adamo, R. Cammi, J. W. Ochterski, R. L. Martin, K. Morokuma, O. Farkas, J. B. Foresman and D. J. Fox in *Gaussian 16 Rev. B.01*, *Vol.* Wallingford, CT, **2016**.
6. a) A.D. Becke, *J.Chem.Phys*. 1993, **98**, 5648; b) C. Lee, W. Yang, R.G. Parr, *Phys. Rev. B* 1988, **37**, 785
7. M. J. Frisch, J. A. Pople and J. S. Binkley, *J. Chem. Phys.,* 1984, **80**, 3265.
8. O.Trott, A. J. Olson, *J. Comput. Chem.* 2010, **31**, 455.